ÉCOLE POLYTECHNIQUE
FÉDÉRALE DE LAUSANNE

MATHICSE
Mathematics Institute of Computational Science and Engineering
School of Basic Sciences - Section of Mathematics

MATHICSE Technical Report
Nr. 36.2012
October 2012


# Isogeometric analysis for second order partial differential equations on surfaces

L. Dedè, A. Quarteroni

http://mathicse.epfl.ch

Phone: +41 21 69 37648

Address:
EPFL - SB - MATHICSE (Bâtiment MA)
Station 8 - CH-1015 - Lausanne - Switzerland

Fax: +41 21 69 32545

# Isogeometric Analyis for second order Partial Differential Equations on surfaces

Luca Dedè [1,*] and Alfio Quarteroni [1,2]

[1] CMCS – Chair of Modeling and Scientific Computing
MATHICSE – Mathematics Institute of Computational Science and Engineering
EPFL – Eć ole Polytechnique Fédérale de Lausanne
Station 8, Lausanne, CH–1015, Switzerland

[2] MOX – Modeling and Scientific Computing
Mathematics Department "F. Brioschi"
Politecnico di Milano
via Bonardi 9, Milano, 20133, Italy

September 28, 2012

**Abstract**

We consider the numerical solution of second order Partial Differential Equations (PDEs) on lower dimensional manifolds, specifically on surfaces in three dimensional spaces. For the spatial approximation, we consider Isogeometric Analysis which facilitates the encapsulation of the exact geometrical description of the manifold in the analysis when this is represented by B–splines or NURBS. Our analysis addresses linear, nonlinear, time dependent, and eigenvalues problems involving the Laplace–Beltrami operator on surfaces. We highlight the accuracy and efficiency of the method with respect to the exactness of the geometrical representations of the surfaces.

**Key words.** Second order Partial Differential Equations; Manifolds; Surfaces; Laplace–Beltrami operator; Isogeometric Analysis.

## 1 Introduction

In several instances, Partial Differential Equations (PDEs) are set up on on lower dimensional manifolds with respect to the hosting physical space, namely on surfaces in three dimensions or curves in two or three–dimensions ([1]). Applications include problems in Fluid Dynamics, Biology, Electromagnetism, and image processing as reported for example in [7, 30, 21, 41, 42]. In addition,

*Corresponding author. E-mail: luca.dede@epfl.ch, Phone:+41 21 6930318, Fax:+41 21 6935510.

PDEs on lower dimensional manifolds could be obtained as reduced mathematical formulations of PDEs defined in thin geometries, e.g. for plates and shells structures [47].

The numerical approximation of these PDEs generally requires the generation of an approximated geometry compatible with the analysis, as it is the case for the Finite Element method (see e.g. [14, 31, 40]). In particular, the approximation of the curvature of surfaces may significantly affect the total error associated to the numerical approximation. Typically, schemes based on the Finite Element method have been used for the approximation of PDEs on surfaces with particular emphasis in controlling and limiting the propagation of the errors associated to the discrete geometrical representation. With this aim, surface Finite Element methods [20, 22] and geometrically consistent Finite Element mesh adaptations [8, 36] have been considered. As alternatives, approaches based on the implicit or immersed surfaces have been proposed, namely based on level set formulations [5, 21] or diffuse interfaces strategies [41]. Still, for a broad range of geometries (surfaces) of practical interest, the above mentioned approaches are not error free in the geometrical representation.

As alternative to these approaches, in this paper we propose numerical approximation of PDEs on lower dimensional manifolds by means of Isogeometric Analysis. Our approach is motivated by the fact that a broad range of geometries of practical interest are exactly represented by B–splines or NURBS ([38]).

Isogeometric Analysis is an approximation method for PDEs based on the isoparametric concept for which the same basis functions used for the geometrical representation are then also used for the numerical approximations of the PDEs [16, 32]. Typically, B–splines or NURBS geometrical representations are considered for Isogeometric Analysis, even if, more recently, T–splines ([44]) have been successfully utilized. Since NURBS are the golden standard in Computer Aided Design (CAD) technology, the use of Isogeometric Analysis facilitates the encapsulation of the exact geometrical representation in the analysis and simplifies the establishment of direct communications between design and numerical approximation of the PDEs. Moreover, NURBS–based Isogeometric Analysis possesses several advantages besides the geometrical considerations, especially in terms of smoothness of the basis functions and accuracy properties [2, 4, 26]. Nowadays, Isogeometric Analysis have been successfully used in a broad range of applications in computational mechanics and optimization, see e.g. [3, 16, 18, 29, 35]. In particular, Isogeometric Analysis have been considered for solving shell problems, as e.g. in [6], and, more recently, Isogeometric Analysis in the framework of the Boundary Element method ([49]) has been used to take advantage of the exact geometrical representation of surfaces [43].

In this work we provide for the first time a general review of the numerical approximation of second order PDEs defined on lower dimensional manifolds described by NURBS, specifically surfaces, by means of Isogeometric Analysis. We discuss the representation of the manifolds in a general framework by means of geometrical mappings from the parameter space to the physical domain; consequently, in view of the use of Isogeometric Analsyis based on the Galerkin method ([40]), we recast the weak forms of the problems and the spatial differential operators in the parameter space. We show the accuracy and efficiency of the method by solving several PDEs endowed with the Laplace–Beltrami spatial operator on surfaces. In particular, as few remarkable instances, we address the numerical solution of the Laplace–Beltrami problem, the eigenvalue problem, a time dependent linear advection–diffusion equation, and the Cahn–Allen phase transition equation ([10, 27]). For both the Laplace–Beltrami and the eigenvalue problems we compare the convergence orders of the errors obtained by means of Isogeometric Analysis with the theoretical ones ([14, 46]) and we highlight the advantages of exactly representing the geometries at the coarsest level of

discretization.

This work is organized as it follows. In Sec. 2 we discuss the representation of lower dimensional manifolds by NURBS and the role of the parametrization in the definition of geometrical mappings. In Sec. 3 we consider the PDEs on the manifolds for problems involving the second order Laplace–Beltrami spatial operator. In Sec. 4 we discuss the numerical approximation schemes, specifically Isogeometric Analysis for the spatial approximation; for the time dependent problems, the generalized–$\alpha$ method ([13]) is considered and a SUPG stabilization scheme ([9]) is presented because of its suitability to treat advection dominated problems. In Sec. 5 we report and discuss the numerical results for PDEs on surfaces. Final considerations are reported in the Conclusions.

# 2 Manifolds represented by NURBS

In this section we introduce in an abstract setting lower dimensional manifolds in the physical space, e.g. curves and surfaces, represented by suitable geometrical mappings. We recall the definition of generic functions and their derivatives on the manifold and we express them in terms of the parametric coordinates upon which the geometrical mapping is built. Finally, we specifically select manifolds defined by B–spline and NURBS and we briefly recall the basics of these geometrical representations.

## 2.1 Manifolds and geometrical mapping

Let us consider a generic (Riemannian) manifold, say $\Omega \subset \mathbb{R}^d$ with $d \geq 1$, defined in the physical space $\mathbb{R}^d$ [1]. Let us assume that the manifold is obtained by means of a geometrical mapping from a parameter space, say $\mathbb{R}^\kappa$, into the physical space $\mathbb{R}^d$, with $d \geq \kappa \geq 1$. If $d > \kappa$ the manifold is lower dimensional with respect to the physical space. More precisely, given a parameter domain, say $\widehat{\Omega} \subset \mathbb{R}^\kappa$, and a vector–valued independent variable $\boldsymbol{\xi} = (\xi_1, \ldots, \xi_\kappa) \in \mathbb{R}^\kappa$, the manifold $\Omega \subset \mathbb{R}^d$ is defined by means of the geometrical mapping:

$$\mathbf{x} \ : \ \widehat{\Omega} \to \mathbb{R}^d, \qquad \boldsymbol{\xi} \to \mathbf{x}(\boldsymbol{\xi}). \tag{2.1}$$

For example, if $d = 3$ and $\kappa = 1$, the manifold $\Omega$ represents a curve in $\mathbb{R}^3$, while if $\kappa = 2$, $\Omega$ is a surface in $\mathbb{R}^3$. Specifically, we consider compact, connected, and oriented manifolds $\Omega$ defined from parameter domains $\widehat{\Omega}$ of finite, positive measure with respect to the topology of $\mathbb{R}^\kappa$ ($0 < |\widehat{\Omega}| < +\infty$).

For the mapping (2.1), we define its Jacobian:

$$\widehat{\mathrm{F}} \ : \ \widehat{\Omega} \to \mathbb{R}^{d\times\kappa}, \qquad \boldsymbol{\xi} \to \widehat{\mathrm{F}}(\boldsymbol{\xi}), \qquad \widehat{\mathrm{F}}_{i,j}(\boldsymbol{\xi}) := \frac{\partial \mathbf{x}_i}{\partial \boldsymbol{\xi}_j}(\boldsymbol{\xi}), \ i = 1, \ldots, d, \ j = 1, \ldots, \kappa. \tag{2.2}$$

We also introduce the first fundamental form of the mapping:

$$\widehat{\mathrm{G}} \ : \ \widehat{\Omega} \to \mathbb{R}^{\kappa\times\kappa}, \qquad \boldsymbol{\xi} \to \widehat{\mathrm{G}}(\boldsymbol{\xi}), \qquad \widehat{\mathrm{G}}(\boldsymbol{\xi}) := \left(\widehat{\mathrm{F}}(\boldsymbol{\xi})\right)^T \widehat{\mathrm{F}}(\boldsymbol{\xi}) \tag{2.3}$$

and finally its determinant:

$$\widehat{g} \ : \ \widehat{\Omega} \to \mathbb{R}, \qquad \boldsymbol{\xi} \to \widehat{g}(\boldsymbol{\xi}), \qquad \widehat{g}(\boldsymbol{\xi}) := \sqrt{\det\left(\widehat{\mathrm{G}}(\boldsymbol{\xi})\right)}. \tag{2.4}$$

We observe that in the case for which $\kappa = d$, then $\widehat{\mathrm{F}}(\boldsymbol{\xi}) \in \mathbb{R}^{d\times d}$ and $\widehat{g}(\boldsymbol{\xi}) \equiv \det\left(\widehat{\mathrm{F}}(\boldsymbol{\xi})\right)$ (when positive). We assume that the geometrical mapping (2.1) is "sufficiently" smooth, e.g. $C^1(\widehat{\Omega})$, and invertible *a.e.* in $\widehat{\Omega}$. Notice that we allow the mapping to be locally not invertible in subdomains $Q$ of $\Omega$ with zero measure in the topology of $\mathbb{R}^\kappa$; specifically, we require that $\widehat{g}(\boldsymbol{\xi}) > 0$ *a.e.* in $\widehat{\Omega}$ with $\widehat{g}(\boldsymbol{\xi}) = 0$ for $\boldsymbol{\xi} \in \widehat{Q} \subset \widehat{\Omega}$ only if $\mathrm{meas}\left(\widehat{Q}\right) \equiv 0$, where $\widehat{Q}$ is the subdomain of $\widehat{\Omega}$ mapping the subdomain $Q$ of $\Omega$.

### 2.2 Functions and differential operators on manifolds

Let assume that a "sufficiently" regular function is defined on the manifold $\Omega$, e.g. $\phi \in C^0(\Omega)$ for all $\mathbf{x} \in \Omega$; then, since we consider invertible geometrical mappings, we can write:

$$\phi(\mathbf{x}) = \widehat{\phi}(\boldsymbol{\xi}) \circ \mathbf{x}^{-1}(\boldsymbol{\xi}), \tag{2.5}$$

where $\widehat{\phi}(\boldsymbol{\xi}) := \phi\left(\mathbf{x}(\boldsymbol{\xi})\right)$. Moreover, we define the gradient on the manifold $\Omega$ of the function $\phi \in C^1(\Omega)$, say $\nabla_\Omega \phi \in \mathbb{R}^d$, as the projection of the gradient operator associated to the physical space onto the manifold. With this aim, we introduce the smooth prolongation of the function $\phi(\mathbf{x})$ from $\widehat{\Omega}$ into a tubular region in $\mathbb{R}^d$ containing $\widehat{\Omega}$ [8, 19], say $\widetilde{\phi}(\mathbf{x})$, and the projector tensor $\mathrm{P}(\mathbf{x}) \in \mathbb{R}^{d\times d}$:

$$\mathrm{P}(\mathbf{x}) := I - \mathbf{n}_\Omega(\mathbf{x}) \otimes \mathbf{n}_\Omega(\mathbf{x}) \qquad \text{for } \mathbf{x} \in \Omega, \tag{2.6}$$

with the unit vector $\mathbf{n}_\Omega(\mathbf{x})$ normal to the manifold $\Omega$ in $\mathbb{R}^d$ and $I$ the identity tensor in $\mathbb{R}^{d\times d}$; in this manner, we have:

$$\nabla_\Omega \phi(\mathbf{x}) := \left[\mathrm{P}(\mathbf{x})\, \nabla \widetilde{\phi}(\mathbf{x})\right] \qquad \text{for } \mathbf{x} \in \Omega. \tag{2.7}$$

For example, for a curve in $\mathbb{R}^d$ we have $\nabla_\Omega \phi(\mathbf{x}) = \left(\nabla \widetilde{\phi}(\mathbf{x}) \cdot \mathbf{t}_\Omega(\mathbf{x})\right) \mathbf{t}_\Omega(\mathbf{x})$, where $\mathbf{t}_\Omega(\mathbf{x})$ is the unit tangent vector to the curve, while for a surface in $\mathbb{R}^d$, we obtain that $\nabla_\Omega \phi(\mathbf{x}) = \nabla \widetilde{\phi}(\mathbf{x}) - \left(\nabla \widetilde{\phi}(\mathbf{x}) \cdot \mathbf{n}_\Omega(\mathbf{x})\right) \mathbf{n}_\Omega(\mathbf{x})$[1]. Finally, we introduce the Laplace–Beltrami operator associated to the manifold $\Omega$ for a function $\phi \in C^2(\Omega)$ as:

$$\Delta_\Omega \phi(\mathbf{x}) := \nabla_\Omega \cdot \left(\nabla_\Omega \phi(\mathbf{x})\right), \tag{2.8}$$

where the divergence operator $\nabla_\Omega \cdot$ is defined as $\nabla_\Omega \cdot \mathbf{v}(\mathbf{x}) = \mathrm{trace}\left[\nabla_\Omega \mathbf{v}(\mathbf{x})\right]$ for all $\mathbf{v} \in \left[C^1(\Omega)\right]^d$. By using the notation of Eq. (2.7), we obtain for the Laplace–Beltrami operator:

$$\Delta_\Omega \phi(\mathbf{x}) = \mathrm{trace}\left[\mathrm{P}(\mathbf{x})\, \nabla^2 \widetilde{\phi}(\mathbf{x})\, \mathrm{P}(\mathbf{x})\right] \qquad \text{for } \mathbf{x} \in \Omega, \tag{2.9}$$

where $\nabla^2 \cdot$ indicates the Hessian operator such that $\left(\nabla^2 \widetilde{\phi}(\mathbf{x})\right)_{i,j} := \dfrac{\partial^2 \widetilde{\phi}}{\partial \mathrm{x}_i \partial \mathrm{x}_j}(\mathbf{x})$.

By using the geometrical mapping (2.1), the gradient on the manifold (2.7) can be rewritten as:

$$\nabla_\Omega \phi(\mathbf{x}) = \left[\widehat{\mathrm{F}}(\boldsymbol{\xi})\, \widehat{\mathrm{G}}^{-1}(\boldsymbol{\xi}) \widehat{\nabla} \widehat{\phi}(\boldsymbol{\xi})\right] \circ \mathbf{x}^{-1}(\boldsymbol{\xi}), \tag{2.10}$$

[1] Notice that for a surface in $\mathbb{R}^3$ the unit normal vector $\mathbf{n}_\Omega(\mathbf{x})$ is obtained by mapping $\widehat{\mathbf{n}}_\Omega(\boldsymbol{\xi}) := \dfrac{\widehat{\mathbf{t}}_{\boldsymbol{\Omega},\mathbf{1}}(\boldsymbol{\xi}) \times \widehat{\mathbf{t}}_{\boldsymbol{\Omega},\mathbf{2}}(\boldsymbol{\xi})}{\|\widehat{\mathbf{t}}_{\boldsymbol{\Omega},\mathbf{1}}(\boldsymbol{\xi}) \times \widehat{\mathbf{t}}_{\boldsymbol{\Omega},\mathbf{2}}(\boldsymbol{\xi})\|}$ with $\widehat{\mathbf{t}}_{\Omega,i}(\boldsymbol{\xi}) := \dfrac{\partial \mathbf{x}}{\partial \boldsymbol{\xi}_i}(\boldsymbol{\xi})$ for $i = 1, 2$.

where $\widehat{\nabla}\widehat{\phi} \ : \ \widehat{\Omega} \to \mathbb{R}^{\kappa}$ is the gradient operator in the parameter space. Similarly, for the Laplace–Beltrami operator of Eq. (2.8), we have ([1]):

$$\Delta_{\Omega}\phi(\mathbf{x}) = \left[\frac{1}{\widehat{g}(\boldsymbol{\xi})}\,\widehat{\nabla}\cdot\left(\widehat{g}(\boldsymbol{\xi})\,\widehat{\mathrm{G}}^{-1}(\boldsymbol{\xi})\,\widehat{\nabla}\widehat{\phi}(\boldsymbol{\xi})\right)\right]\circ\mathbf{x}^{-1}(\boldsymbol{\xi}). \tag{2.11}$$

Finally, in view of the definitions of integrals in the weak form of the PDEs, the differential $d\mathbf{x}$ (or $d\Omega$) can be written as $d\mathbf{x} = \widehat{g}(\boldsymbol{\xi})\,d\boldsymbol{\xi}$ (or $d\Omega = \widehat{g}(\boldsymbol{\xi})\,d\widehat{\Omega}$).

### 2.3 Geometrical mapping by NURBS

We assume that the geometrical mapping introduced in Eq. (2.1) defines a manifold $\Omega$ represented by either B–splines or NURBS; for a detailed description we refer the reader to [38]. We observe that in the framework of Isogeometric Analysis, the choice of T–splines [44] represents a valid alternative and generalization.

The geometrical mapping (2.1) represented in terms of NURBS reads:

$$\mathbf{x}(\boldsymbol{\xi}) = \sum_{i=1}^{n_{bf}} \widehat{R}_i(\boldsymbol{\xi})\,\mathbf{P}_i, \tag{2.12}$$

where $\widehat{R}_i(\boldsymbol{\xi})$ are the NURBS basis functions defined in the parameter domain $\widehat{\Omega}$ and $\mathbf{P}_i \in \mathbb{R}^d$ are the control points in the physical space for $i = 1, \ldots, n_{bf}$. The NURBS basis functions $\widehat{R}_i(\boldsymbol{\xi})$ are defined from B–splines basis functions $\widehat{N}_i(\boldsymbol{\xi})$ and weights $w_i \in \mathbb{R}$ as:

$$\widehat{R}_i(\boldsymbol{\xi}) := \frac{w_i}{\displaystyle\sum_{i'=1}^{n_{bf}} w_{i'}\,\widehat{N}_{i'}(\boldsymbol{\xi})}\,\widehat{N}_i(\boldsymbol{\xi}) \qquad \text{for } i = 1, \ldots, n_{bf}; \tag{2.13}$$

we observe that B–splines geometries in $\mathbb{R}^d$ can be seen as a particular case of NURBS with weights equal to the unity[2]. The (multivariate) B–splines basis functions $\widehat{N}_i(\boldsymbol{\xi})$ are obtained by tensor product rule of univariate B–splines basis functions, say $\widehat{N}_{k,i}(\xi_k)$ for $i = 1, \ldots, n_{bf,k}$, where $k = 1, \ldots, \kappa$ indicates the parametric direction $\xi_k$ in $\mathbb{R}^{\kappa}$ with $\boldsymbol{\xi} = (\xi_1, \ldots, \xi_{\kappa})$ and $n_{bf} = \Pi_{k=1}^{\kappa} n_{bf,k}$. The univariate B–spline basis functions $\widehat{N}_{k,i}(\xi_k)$ are recursively built by using the Cox–de Boor recursion formula starting from a knot vector $\Xi_k := \{\xi_{k,j}\}_{j=1}^{n_{bf,k}+p_k+1}$ with $\xi_{k,j} \in \mathbb{R}$ which, together with the polynomial order $p_k$, completely characterizes the properties of the basis functions. We observe that the parameter domain $\widehat{\Omega}$ is obtained by the knot vectors as $\widehat{\Omega} = (\xi_{1,1}, \xi_{n_{bf,1}+p_1+1}) \times \cdots \times (\xi_{\kappa,1}, \xi_{n_{bf,\kappa}+p_{\kappa}+1})$. The tensor product of the knots also defines a partition of the domain $\widehat{\Omega}$ into subdomains $\Omega_e$, for $e = 1, \ldots, n_{el}$, which we regard as "mesh" elements, $n_{el}$ being their number. The geometrical mapping of the elements $\widehat{\Omega}_e$ into the physical space defines the elements $\Omega_e$, for $e = 1, \ldots, n_{el}$.

For example, in Fig. 1 we report open–knot, univariate B–spline basis functions of order $p = 1, 2, 3$ obtained by the knot vectors $\Xi = \left\{\{0\}^{p+1}, \frac{1}{5}, \frac{2}{5}, \frac{3}{5}, \frac{4}{5}, \{1\}^{p+1}\right\}$, respectively; we observe that the basis functions are globally $C^{p-1}$ continuous in $\widehat{\Omega} = (0, 1)$ for this specific choice of the knot vector. In Fig. 2 we report two examples of surfaces in $\mathbb{R}^3$ obtained by NURBS, a cylindrical and

[2]NURBS are obtained by projective transformations of B–splines defined in the physical space $\mathbb{R}^{d+1}$.

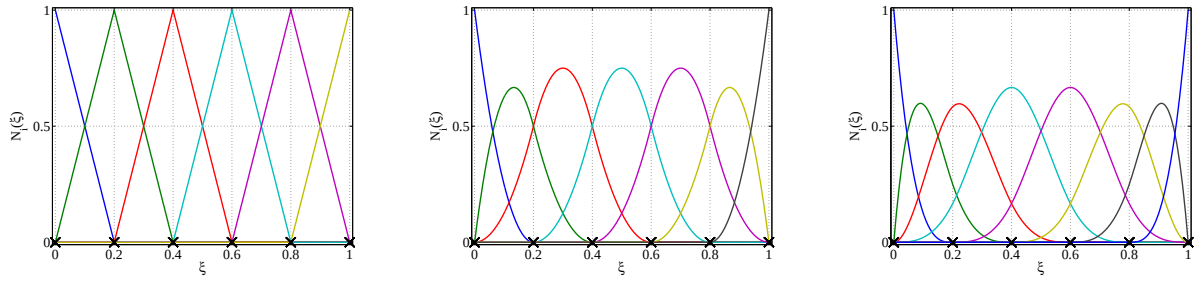


$p = 1$ $p = 2$ $p = 3$

Figure 1: Univariate, globally $C^{p-1}$–continuous, B–spline basis functions $\left\{\widehat{N}_i(\xi)\right\}_{i=1}^{n}$ of order $p = 1, 2$, and 3 obtained by the knot vectors $\Xi = \left\{\{0\}^{p+1}, \frac{1}{5}, \frac{2}{5}, \frac{3}{5}, \frac{4}{5}, \{1\}^{p+1}\right\}$, respectively; $\widehat{\Omega} = (0, 1)$.

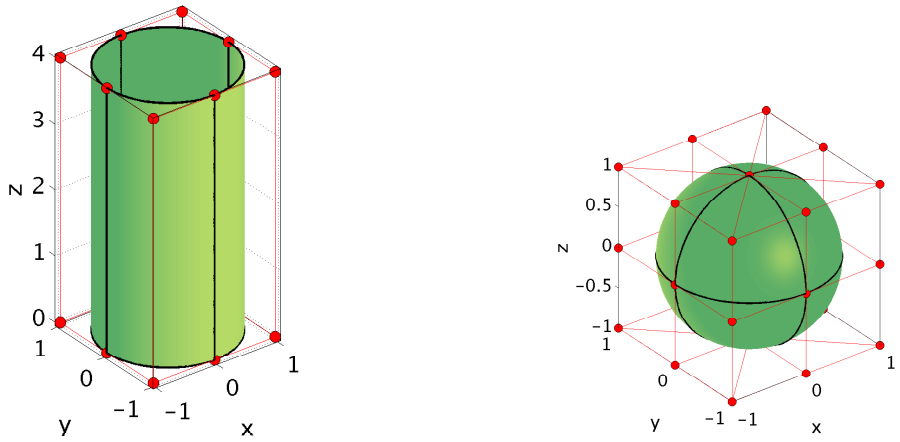


Figure 2: NURBS surfaces $\Omega$ in $\mathbb{R}^3$: cylindrical shell of radius 1 and height 4 (left) and spherical shell of radius 1 (right). The "mesh" elements are highlighted in black, the control net and control points $\{\mathbf{P}_i\}_{i=1}^{n}$, in red.

a spherical shell (we refer the reader to e.g. [16] and [38] for the construction of these geometries). We observe that both the geometries are exactly represented by NURBS at the coarsest level of discretization ($n_{el} = 4$ and 8 "mesh elements" and $n_{bf} = 18$ and 45 basis functions for the cylinder and the sphere, respectively).

In several circumstances, more complicated geometries can be generated by combining multiple NURBS patches.

## 3 PDEs on the manifold

With the aim of generality, we introduce a nonlinear parabolic PDE with second order spatial derivatives, corresponding to the Laplace–Beltrami operator. Then, as particular cases of such general PDE, we present the equations we will address in this work, namely: an elliptic PDE, an

eigenvalue problem, a time dependent advection–diffusion equation and the Cahn–Allen equation defined on the manifold. Then, in view of the numerical approximation, we rewrite the weak form of the equations in the parametric space by means of the geometrical mapping introduced in Sec. 2.

### 3.1 The nonlinear parabolic PDE with Laplace–Beltrami operator

Let us denote with $\Gamma = \partial\Omega$ the boundary of the manifold $\Omega$; then we say that $\Omega$ possesses a boundary if $\text{meas}(\Gamma) \neq 0$ in the topology of $\mathbb{R}^{\kappa-1}$; for example, by referring to Fig. 2(left), the cylindrical shell has a boundary $\Gamma = \left\{\mathbf{x} = (\mathrm{x},\mathrm{y},\mathrm{z}) \in \mathbb{R}^3 \ : \ \mathrm{x}^2 + \mathrm{y}^2 = 1 \text{ and } \mathrm{z} = \{0,4\}\right\}$, while the sphere does not posses a boundary ($\text{meas}(\Gamma) = 0$). If $\text{meas}(\Gamma) \neq 0$, then we can partition it into two non overlapping subdomains, say $\Gamma_D$ and $\Gamma_N$, such that $\overline{\Gamma_D \bigcup \Gamma_N} \equiv \Gamma$ and $\overset{\circ}{\Gamma}_D \bigcap \overset{\circ}{\Gamma}_N = \emptyset$.

For the sake of simplicity and unless when necessary for clarity, we will omit from here on the explicit dependence of the functions defined in the physical space $\mathbb{R}^d$ on the spatial variable $\mathbf{x}$ and, similarly, for the functions in the parameter space $\mathbb{R}^\kappa$, the explicit dependence on the independent variable $\boldsymbol{\xi}$.

By recalling the definition of the Laplace–Beltrami operator (2.8), we assume the following expression for the time dependent nonlinear parabolic PDE, where $u(t)$ represents its solution:

$$\begin{aligned}
&\alpha\frac{\partial u}{\partial t}(t) - \mu\Delta_\Omega u(t) + \mathbf{V}\cdot\nabla_\Omega u(t) + \sigma\left(u(t)\right) = f && \text{in } \Omega\times(0,T),\\
&u(t) = \gamma && \text{on } \Gamma_D\times(0,T),\\
&\mu\nabla_\Omega u(t)\cdot\mathbf{n}_\Gamma = 0 && \text{on } \Gamma_N\times(0,T),\\
&u(0) = u_{in} && \text{in } \Omega\times\{0\},
\end{aligned} \tag{3.1}$$

where $T > 0$ is the final time and $\mathbf{n}_\Gamma$ is the unit vector normal to the boundary $\Gamma$ (note that $\mathbf{n}_\Gamma\cdot\mathbf{n}_\Omega = 0$ for all $\mathbf{x}\in\Gamma$). For simplicity, the coefficients $\alpha \geq 0$ and $\mu > 0$ are assumed as constants in $\mathbb{R}$, the advection field $\mathbf{V} \in [L^\infty(\Omega)]^d$ is such that $\mathbf{V}\cdot\mathbf{n}_\Omega = 0$, $\nabla_\Omega\cdot\mathbf{V} \in L^2(\Omega)$ and $\nabla_\Omega\cdot\mathbf{V} = 0$ *a.e.* for $\mathbf{x}\in\Omega$, and the source term $f \in L^2(\Omega)$; the reaction term $\sigma(u(t))$ is assumed "sufficiently" regular, i.e. as $\sigma(u(t)) \in L^\infty(\Omega\times(0,T))$. Moreover, $\gamma \in H^{1/2}(\Gamma_D)$, and the initial condition $u_{in} \in L^2(\Omega)$; for the sake of simplicity, we assumed an homogeneous Neumann condition on $\Gamma_N$. We observe that, if the manifold $\Omega$ does not possesses a boundary ($\text{meas}(\Gamma) = 0$), the boundary conditions in Eq. (3.1) become meaningless and they should be replaced by other conditions on the solution $u(t)$ depending on the choice of the data (see Sec. 3.2).

In view of the weak form of the problem (3.1), we introduce the function spaces $\mathcal{V}_\gamma$ and $\mathcal{V}$ as:

$$\mathcal{V}_\gamma := \left\{v \in H^1(\Omega) \ : \ v|_{\Gamma_D} = \gamma\right\}, \qquad \mathcal{V} := \left\{v \in H^1(\Omega) \ : \ v|_{\Gamma_D} = 0\right\}. \tag{3.2}$$

Moreover, we introduce the following forms and functionals:

$$\begin{aligned}
&a(v,w) := \int_\Omega \mu\,\nabla_\Omega v\cdot\nabla_\Omega w\,d\Omega, && b(v,w) := \int_\Omega v\,\mathbf{V}\cdot\nabla_\Omega w\,d\Omega,\\
&c(w)(v) := \int_\Omega v\,\sigma(w)\,d\Omega, && m(v,w) := \int_\Omega v\,w\,d\Omega,\\
&q(v) := \int_\Omega v\,f\,d\Omega,
\end{aligned} \tag{3.3}$$

and the weak residual:

$$\begin{aligned} Res\,(w(t))\,(v) \;&:=\; q(v) - a(v(t), w(t)) - b(v, w(t)) \\ &\quad -c(w(t))(v) - \alpha\, m\left(v, \frac{\partial w}{\partial t}(t)\right), \end{aligned} \tag{3.4}$$

for any $v \in \mathcal{V}$, $w(t) \in \mathcal{V}_\gamma$, for all $t \in (0,T)$. Then, the weak form of the problem (3.1) reads:

$$\begin{aligned} &\text{find } u(t) \in \mathcal{V}_\gamma \;:\; Res\,(u(t))\,(v) = 0 \qquad \forall v \in \mathcal{V},\ \forall t \in (0,T), \\ &\text{with } u(0) = u_{in}. \end{aligned} \tag{3.5}$$

We shall assume that the above problem is well–posed; for example, we observe that for $\alpha = 1$, $\mathbf{V} = \mathbf{0}$, and $\sigma(u(t)) = \sigma_0\, u(t)$ for some $\sigma_0 > 0$, under the regularity hypothesis on the other data, we have a unique solution $u(t) \in L^2\left((0,T); \mathcal{V}_\gamma\right) \cap C^0\left((0,T); L^2(\Omega)\right)$ by using similar arguments of [40]. For further details see e.g. [15, 23, 24, 25].

With the aim of writing the problem (3.5) in the parameter space, we recall the mapping of the data based on Eqs. (2.1) and (2.5). In particular, we have: $\widehat{\mathbf{V}}(\boldsymbol{\xi}) := \mathbf{V}(\mathbf{x}(\boldsymbol{\xi}))$, $\widehat{f}(\boldsymbol{\xi}) := f(\mathbf{x}(\xi))$, $\widehat{\gamma}(\boldsymbol{\xi}) := \gamma(\mathbf{x}(\boldsymbol{\xi}))$, and $\widehat{u}_{in}(\boldsymbol{\xi}) := u_{in}(\mathbf{x}(\xi))$; we notice that $\widehat{\sigma}(\cdot) \equiv \sigma(\cdot)$. Moreover, we introduce the function spaces $\widehat{\mathcal{V}}_\gamma$ and $\widehat{\mathcal{V}}$ as:

$$\widehat{\mathcal{V}}_\gamma := \left\{\widehat{v} \in H^1(\widehat{\Omega}) \;:\; \widehat{v}|_{\widehat{\Gamma}_D} = \widehat{\gamma}\right\}, \qquad \widehat{\mathcal{V}} := \left\{\widehat{v} \in H^1(\widehat{\Omega}) \;:\; \widehat{v}|_{\widehat{\Gamma}_D} = 0\right\}, \tag{3.6}$$

where, if $\mathrm{meas}\,(\Gamma) \neq 0$, $\widehat{\Gamma}_D := \left\{\boldsymbol{\xi} \in \partial\widehat{\Omega} \;:\; \mathbf{x}(\boldsymbol{\xi}) \in \Gamma_D\right\}$ and $\widehat{\Gamma}_N = \partial\widehat{\Omega}\backslash\widehat{\Gamma}_D$. Also, we introduce the following forms and functionals from Eqs. (2.5), (2.10) and (3.3):

$$\begin{aligned} &\widehat{a}(\widehat{v}, \widehat{w}) := \int_{\widehat{\Omega}} \mu\, \widehat{\nabla}\widehat{v} \cdot \left(\widehat{\mathrm{G}}^{-1}\, \widehat{\nabla}\widehat{w}\right)\, \widehat{g}\, d\widehat{\Omega}, && \widehat{b}(\widehat{v}, \widehat{w}) := \int_{\widehat{\Omega}} \widehat{v}\, \widehat{\mathbf{V}} \cdot \left(\widehat{\mathrm{F}}\, \widehat{\mathrm{G}}^{-1}\, \widehat{\nabla} w\right)\, \widehat{g}\, d\widehat{\Omega}, \\ &\widehat{c}(\widehat{w})(\widehat{v}) := \int_{\widehat{\Omega}} \widehat{v}\, \widehat{\sigma}(\widehat{w})\, \widehat{g}\, d\widehat{\Omega}, && \widehat{m}(\widehat{v}, \widehat{w}) := \int_{\widehat{\Omega}} \widehat{v}\, \widehat{w}\, \widehat{g}\, d\widehat{\Omega}, \\ &\widehat{q}(\widehat{v}) := \int_{\widehat{\Omega}} \widehat{v}\, \widehat{f}\, \widehat{g}\, d\widehat{\Omega}, \end{aligned} \tag{3.7}$$

and the weak residual:

$$\widehat{Res}\,(\widehat{w}(t))\,(\widehat{v}) := \widehat{q}(\widehat{v}) - \widehat{a}(\widehat{v}, \widehat{w}(t)) - \widehat{b}(\widehat{v}, \widehat{w}(t)) - \widehat{c}(\widehat{w}(t))(\widehat{v}) - \alpha\, \widehat{m}\left(\widehat{v}, \frac{\partial \widehat{w}}{\partial t}(t)\right), \tag{3.8}$$

for any $\widehat{v} \in \widehat{\mathcal{V}}$, $\widehat{w}(t) \in \widehat{\mathcal{V}}_\gamma$, and for all $t \in (0,T)$. Finally, the weak form of the problem (3.5) in the parameter space reads:

$$\begin{aligned} &\text{find } \widehat{u}(t) \in \widehat{\mathcal{V}}_\gamma \;:\; \widehat{Res}\,(\widehat{u}(t))\,(\widehat{v}) = 0 \qquad \forall \widehat{v} \in \widehat{\mathcal{V}},\ \forall t \in (0,T), \\ &\text{with } \widehat{u}(0) = \widehat{u}_{in}; \end{aligned} \tag{3.9}$$

we observe that, from Eq. (2.5), we have $u(\mathbf{x}, t) = \widehat{u}(\boldsymbol{\xi}, t) \circ \mathbf{x}^{-1}(\boldsymbol{\xi})$ and $\widehat{u}(\boldsymbol{\xi}, t) = u(\mathbf{x}(\boldsymbol{\xi}), t)$ for all $t \in (0,T)$.

### 3.2 The Laplace–Beltrami equation

By referring to Eq. (3.1) and assuming the data and solution $u$ as time independent, $\alpha = 0$, $\mathbf{V} = \mathbf{0}$, and $\sigma(u) = 0$, we obtain the Laplace–Beltrami problem:

$$\text{find } u \in \mathcal{V}_\gamma \ : \ a(v,u) = q(v) \qquad \forall v \in \mathcal{V}, \tag{3.10}$$

for some $\mu > 0$. We observe that, if the manifold $\Omega$ is not endowed with a boundary, then the Laplace–Beltrami problem (3.10) is ill–posed. For this reason, if $\text{meas}\,(\Gamma) = 0$, the solution space $\mathcal{V}_\gamma$ is replaced e.g. by the space $\mathcal{V}_0 := \left\{ v \in H^1(\Omega) \ : \ \displaystyle\int_\Omega v \, d\Omega = 0 \right\}$ (see e.g. [37]).

By recasting problem (3.10) in the parameter space, we obtain:

$$\text{find } \widehat{u} \in \widehat{\mathcal{V}}_\gamma \ : \ \widehat{a}(\widehat{v},\widehat{u}) = \widehat{q}(\widehat{v}) \qquad \forall \widehat{v} \in \widehat{\mathcal{V}}, \tag{3.11}$$

where we have used the notation introduced in Sec. 3.1.

### 3.3 The Eigenvalue problem

From Eq. (3.1), by assuming that the data and solution $u$ are time independent, and setting $\alpha = 0$, $\mathbf{V} = \mathbf{0}$, and $\sigma(u) = -\lambda\, u$, assuming the parameter $\lambda$ as unknown, we obtain the Laplace–Beltrami eigenvalue problem[3]:

$$\text{find } u \in \mathcal{V} \text{ and } \lambda \in \mathbb{R} \ : \ a(v,u) = \lambda\, m(v,u) \qquad \forall v \in \mathcal{V}; \tag{3.12}$$

specifically, we set $\mu = 1$. We observe that, since the problem is symmetric, the eigenvalues are real valued, i.e. $\lambda \in \mathbb{R}$, with $\lambda \geq 0$.

In the parameter space, Eq. (3.12) reads:

$$\text{find } \widehat{u} \in \widehat{\mathcal{V}} \text{ and } \lambda \in \mathbb{R} \ : \ \widehat{a}(\widehat{v},\widehat{u}) = \lambda\, \widehat{m}(\widehat{v},\widehat{u}) \qquad \forall \widehat{v} \in \widehat{\mathcal{V}}. \tag{3.13}$$

### 3.4 The time dependent linear advection–diffusion equation

By using the notation of Sec. 3.1, we introduce the parabolic linear advection–diffusion equation in the following weak form:

$$\begin{aligned} &\text{find } u(t) \in \mathcal{V}_\gamma \ : \ m\left(v, \frac{\partial u}{\partial t}(t)\right) + a(v,u(t)) + b(v,u(t)) = q(v) \qquad \forall v \in \mathcal{V}, \ \forall t \in (0,T), \\ &\text{with } u(0) = u_{in}, \end{aligned} \tag{3.14}$$

where we set $\sigma(u(t)) = 0$ and $\alpha = 1$. In view of the numerical approximation, we introduce the following operators, say $\mathcal{L}(\cdot)$ and $\mathcal{L}_{adv}(\cdot)$, as:

$$\mathcal{L}(w(t)) := \frac{\partial w}{\partial t}(t) - \mu\, \Delta_\Omega w(t) + \mathbf{V} \cdot \nabla_\Omega w(t), \tag{3.15}$$

$$\mathcal{L}_{adv}(w(t)) := \mathbf{V} \cdot \nabla_\Omega w(t), \tag{3.16}$$

and the strong residual $\mathcal{R}(\cdot)$ in $\Omega$ as:

$$\mathcal{R}\,(w(t)) := f - \mathcal{L}(w(t)), \tag{3.17}$$

[3] For $\sigma(u) = -\lambda\, u$, the form $c(\cdot)(\cdot)$ in Eq. (3.3) reads $c(w)(v) = -\lambda\, m(v,u)$ for any $v(\mathbf{x})$, $w(t) \in \mathcal{V}$.

for all $w(t) \in H^2(\Omega)$ for any $t \in (0,T)$.

In the parameter space, Eq. (3.14) reads:

$$\begin{aligned} &\text{find } \widehat{u}(t) \in \widehat{\mathcal{V}}_\gamma \ : \ \widehat{m}\left(\widehat{v}, \frac{\partial \widehat{u}}{\partial t}(t)\right) + \widehat{a}(\widehat{v}, \widehat{u}(t)) + \widehat{b}(\widehat{v}, \widehat{u}(t)) = \widehat{q}(\widehat{v}) \qquad \forall \widehat{v} \in \widehat{\mathcal{V}}, \ \forall t \in (0,T), \\ &\text{with } \widehat{u}(0) = \widehat{u}_{in}, \end{aligned} \tag{3.18}$$

while the operators and the residual in Eqs. (3.15), (3.16), and (3.17) are:

$$\widehat{\mathcal{L}}(\widehat{w}(t)) := \frac{\partial \widehat{w}}{\partial t}(t) - \mu \frac{1}{\widehat{g}} \widehat{\nabla} \cdot \left(\widehat{g}\, \widehat{\mathrm{G}}^{-1}\, \widehat{\nabla} \widehat{w}(t)\right) + \widehat{\mathbf{V}} \cdot \left(\widehat{\mathrm{F}}\, \widehat{\mathrm{G}}^{-1}\, \widehat{\nabla} \widehat{w}(t)\right), \tag{3.19}$$

$$\widehat{\mathcal{L}}_{adv}(\widehat{w}(t)) := \widehat{\mathbf{V}} \cdot \left(\widehat{\mathrm{F}}\, \widehat{\mathrm{G}}^{-1}\, \widehat{\nabla} \widehat{w}(t)\right), \tag{3.20}$$

$$\widehat{\mathcal{R}}\,(\widehat{w}(t)) := \widehat{f} - \widehat{\mathcal{L}}(\widehat{w}(t)), \tag{3.21}$$

for all $\widehat{w}(t) \in H^2(\widehat{\Omega})$ for any $t \in (0,T)$.

### 3.5 The Cahn–Allen equation

By denoting with $u(t)$ the concentration of a component of a binary isothermal mixture, we describe its evolution in time by means of the Cahn–Allen equation, a nonlinear, time dependent PDE. For further details on the topic we refer the reader e.g. to [10, 11, 12, 27]. The Cahn–Allen equation in weak form reads:

$$\begin{aligned} &\text{find } u(t) \in \mathcal{V} \ : \ m\left(v, \frac{\partial u}{\partial t}(t)\right) + a(v, u(t)) + c(u(t))(v) = 0 \qquad \forall v \in \mathcal{V}, \ \forall t \in (0,T), \\ &\text{with } u(0) = u_{in}, \end{aligned} \tag{3.22}$$

where we set $\sigma(u(t)) = \Psi_{c,u}(u(t)) = 2u(t)\,(u(t)-1)\,(2u(t)-1)$ (for which we have that $c(u(t))(v) = \displaystyle\int_\Omega v\, \Psi_{c,u}(u(t))\, d\Omega$), $\mathbf{V} = \mathbf{0}$, $\alpha = 1$, and $f = 0$. Moreover, if $\mathrm{meas}\,(\Gamma) \neq 0$, we set $\Gamma_N \equiv \Gamma$ with $\Gamma_D = \emptyset$. The Cahn–Allen equation (3.22) represents the gradient flow in the $L^2(\Omega)$ norm of the following energy functional (total free energy) for isothermal binary mixtures on surfaces:

$$\widetilde{\Psi}(t) = \Psi(u(t)) := \int_\Omega \left(\Psi_c(u(t)) + \frac{1}{2}\,\mu\,|\nabla_\Omega u(t)|^2\right) d\Omega, \tag{3.23}$$

where $\Psi_c(\cdot)$ is the chemical energy, which, in this specific case, we have choosen as $\Psi_c(u(t)) = (u(t))^2\,(u(t)-1)^2$; the functional $\Psi_{c,u}(\cdot) = \sigma(\cdot)$ represents the chemical potential and is obtained as the Frechét derivative of $\Psi_c(\cdot)$ with respect to the variable $u(t)$. The free energy $\widetilde{\Psi}(t)$ represents a Liapunov functional since $\dfrac{d\widetilde{\Psi}}{dt}(t) \leq 0$ for all $t \in (0,T]$, being $\nabla_\Omega u(t) \cdot \widehat{\mathbf{n}}_\Gamma = 0$ on $\Gamma$.

In the parameter space, the Cahn–Allen equation reads:

$$\begin{aligned} &\text{find } \widehat{u}(t) \in \widehat{\mathcal{V}} \ : \ \widehat{m}\left(\widehat{v}, \frac{\partial \widehat{u}}{\partial t}(t)\right) + \widehat{a}(\widehat{v}, \widehat{u}(t)) + \widehat{c}(\widehat{u}(t))(\widehat{v}) = 0 \qquad \forall \widehat{v} \in \widehat{\mathcal{V}}, \ \forall t \in (0,T), \\ &\text{with } \widehat{u}(0) = \widehat{u}_{in}, \end{aligned} \tag{3.24}$$

with the free energy:

$$\widetilde{\Psi}(t) = \widehat{\Psi}(u(t)) := \int_{\widehat{\Omega}} \left(\Psi_c(\widehat{u}(t)) + \frac{1}{2}\,\mu\,\widehat{\nabla}\widehat{u}(t) \cdot \left(\widehat{\mathrm{G}}^{-1}\,\widehat{\nabla}\widehat{u}(t)\right)\right) \widehat{g}\, d\widehat{\Omega}, \tag{3.25}$$

being $\widehat{\Psi}_c(\cdot) \equiv \Psi_c(\cdot)$.

# 4 Numerical approximation

In this section we describe the numerical approximation of the PDEs introduced in Sec. 3.1 and represented in compact form in Eq. (3.5). We discuss the approximation in a general setting, firstly for the spatial approximation by means of Isogeometric Analysis and then, for time discretization, the generalized–$\alpha$ method.

## 4.1 The spatial approximation: Isogeometric Analysis

For the spatial approximation of the general problem (3.5) we consider Isogeometric Analysis. In this section we briefly recall the basic notions of the approximation in the framework of the Galerkin method. For further details we refer the reader to [16, 32].

Isogeometric Analysis represents a method for the spatial approximation of PDEs, based on the isoparametric concept for which the same basis used to represent the known geometry are then used to approximate the unknown solution of the PDEs. NURBS or B–splines geometries (computational domains) are represented by geometrical mappings in the form (2.12) from a parameter space to the physical space. By using the isogeometric paradigm, we can define functions in the parameter space in the form:

$$\widehat{u}_h(\boldsymbol{\xi}, t) := \sum_{i=1}^{n_{bf}} \widehat{R}_i(\boldsymbol{\xi})\, U_i(t), \tag{4.1}$$

where $\widehat{R}_i(\boldsymbol{\xi})$ are the NURBS (or B–splines) basis functions (see Eq. (2.13)) and $U_i(t) \in \mathbb{R}$ are the control variables (in fact, the problem unknowns) for $i = 1, \ldots, n_{bf}$, with $n_{bf}$ the number of basis functions; for time dependent problems, the control variables $U_i(t)$ are time dependent. Since the geometrical mapping (2.12) is invertible (as discussed in Secs. 2.1 and 2.3)), we can indifferently refer to functions in the parameter space or in the physical one; from Eq. (2.5) we have $u_h(\mathbf{x}, t) = \widehat{u}_h(\boldsymbol{\xi}, t) \circ \mathbf{x}^{-1}(\boldsymbol{\xi})$. For this reason, we will henceforth consider formulations in the parameter space.

We introduce the finite dimensional function spaces $\widehat{\mathcal{V}}_{\gamma,h} \subset \widehat{\mathcal{V}}_\gamma$ and $\widehat{\mathcal{V}}_h \subset \widehat{\mathcal{V}}$ from Eqs. (3.6) and (4.1); for simplicity, we assume that the data $\widehat{\gamma}$ belongs to the space $\widehat{\mathcal{V}}_h$. Then, the weak form of the problem (3.9) approximated by Isogeometric Analysis reads:

$$\begin{aligned} &\text{find } \widehat{u}_h(t) \in \widehat{\mathcal{V}}_{\gamma,h} \ : \ \widehat{Res}\,(\widehat{u}_h(t))\,(\widehat{v}_h) = 0 \qquad \forall \widehat{v}_h \in \widehat{\mathcal{V}}_h,\ \forall t \in (0,T), \\ &\text{with } \widehat{u}_h(0) = \widehat{u}_{in,h}, \end{aligned} \tag{4.2}$$

where $\widehat{u}_{in,h}$ is the $L^2(\Omega)$ projection of $\widehat{u}_{in}$ onto $\widehat{\mathcal{V}}_h$. The spatial approximation of the problems described in Secs. 3.2, 3.4, and 3.5 fit the general formulation of Eq. (4.2), while the eigenvalue problem (3.13) reads:

$$\text{find } \widehat{u}_h \in \widehat{\mathcal{V}}_h \text{ and } \lambda_h \in \mathbb{R} \ : \ \widehat{a}(\widehat{v}_h, \widehat{u}_h) = \lambda_h\, \widehat{m}(\widehat{v}_h, \widehat{u}_h) \qquad \forall \widehat{v}_h \in \widehat{\mathcal{V}}_h. \tag{4.3}$$

We remark that the function spaces $\widehat{\mathcal{V}}_{\gamma,h}$ and $\widehat{\mathcal{V}}_h$ can be "enriched" by performing $h$– or $p$–refinement of the geometric representation while identically preserving the geometrical mapping[4]. The refinements allow to improve the accuracy of the approximate solution, while still representing

[4]The $h$– or $p$–refinements correspond to the mesh refinement and order elevation procedures of the Finite Element or Spectral methods

exactly the NURBS geometries defining the computational domain. A type of refinement called $k$–refinement and specific for NURBS basis functions can be eventually used to efficiently improve the accuracy by increasing the order $p$ of the basis functions and their global continuity $k$ across the elements $\widehat{\Omega}_e$ in $\widehat{\Omega}$ while containing the number of basis functions $n_{bf}$. For further details we refer the reader to [2, 4, 16, 17, 32].

We remark that numerical integration is performed by means of a quadrature formula with $(p+1)^\kappa$ quadrature points in each element; a direct method ([39]) is considered for the solution of the linear system associated to Eq. (4.2).

### 4.2 The time discretization scheme

For the approximation of time dependent problems, we consider the generalized–$\alpha$ method, a predictor–multicorrector numerical scheme, which we briefly recall in this section; for further details see also e.g. [13, 34].

Let start by introducing a partition of the time interval $(0,T)$ into time steps $\{t_n\}_{n=0}^{n_{ts}}$, where $t_0 = 0$ and $t_{n_{ts}} = T$, with time steps $\Delta t_n := t_{n+1} - t_n$ for $n = 0, \dots, t_{n_{ts}-1}$. Also, we define $\mathbf{U}(t) := \{U_i(t)\}_{i=1}^{n_{bf}}$, $\dot{\mathbf{U}}(t) := \left\{\dot{U}_i(t)\right\}_{i=1}^{n_{bf}}$, $\widehat{\mathbf{Res}}\left(\dot{\mathbf{U}}(t), \mathbf{U}(t)\right) := \left\{\widehat{Res}\left(\widehat{u}_h(t)\right)\left(\widehat{R}_i\right)\right\}_{i=1}^{n_{bf}}$ from Eq. (3.8), $\mathbf{U}_n := \mathbf{U}(t_n)$, and $\dot{\mathbf{U}}_n := \dot{\mathbf{U}}(t_n)$. By introducing the parameters $\alpha_m$, $\alpha_f$, and $\delta \in \mathbb{R}$, the generalized–$\alpha$ method consists in solving the following problem at the time step $t_{n+1}$ given $\dot{\mathbf{U}}_n$ and $\mathbf{U}_n$:

$$\begin{aligned}
&\text{find } \dot{\mathbf{U}}_{n+1}, \mathbf{U}_{n+1}, \dot{\mathbf{U}}_{n+\alpha_m}, \mathbf{U}_{n+\alpha_f} \ : \ \widehat{\mathbf{Res}}\left(\dot{\mathbf{U}}_{n+\alpha_m}, \mathbf{U}_{n+\alpha_f}\right) = \mathbf{0}, \\
&\text{with: } \mathbf{U}_{n+1} = \mathbf{U}_n + \Delta t_n \left((1-\delta)\,\dot{\mathbf{U}}_n + \delta\,\dot{\mathbf{U}}_{n+1}\right), \\
&\qquad \dot{\mathbf{U}}_{n+\alpha_m} = (1-\alpha_m)\,\dot{\mathbf{U}}_n + \alpha_m\,\dot{\mathbf{U}}_{n+1}, \qquad \mathbf{U}_{n+\alpha_f} = (1-\alpha_f)\,\mathbf{U}_n + \alpha_f\,\mathbf{U}_{n+1}.
\end{aligned} \tag{4.4}$$

The previous problem is solved iteratively with $\mathbf{U}_{n+1}$ obtained as $\mathbf{U}_{n+1,(j)}$ for some $j = 0, \dots, j_{max}$ (with $j_{max} > 1$). In particular, at the predictor stage ($j = 0$), we set:

$$\dot{\mathbf{U}}_{n+1,(0)} = \frac{\delta - 1}{\delta}\,\dot{\mathbf{U}}_n, \qquad \mathbf{U}_{n+1,(0)} = \mathbf{U}_n. \tag{4.5}$$

At the multicorrector stage, we repeat for $j = 1, \dots, j_{max}$ the following steps:

1. evaluate the variables:

$$\dot{\mathbf{U}}_{n+\alpha_m,(j)} = (1-\alpha_m)\,\dot{\mathbf{U}}_n + \alpha_m\,\dot{\mathbf{U}}_{n+1,(j-1)}, \qquad \mathbf{U}_{n+\alpha_f,(j)} = (1-\alpha_f)\,\mathbf{U}_n + \alpha_f\,\mathbf{U}_{n+1,(j-1)}; \tag{4.6}$$

2. assemble the residual vector and tangent matrix:

$$\begin{aligned}
&\widehat{\mathbf{Res}}_{n+1,(j)} := \widehat{\mathbf{Res}}\left(\dot{\mathbf{U}}_{n+\alpha_m,(j)}, \mathbf{U}_{n+\alpha_f,(j)}\right), \\
&\widehat{\mathbf{K}}_{n+1,(j)} := \alpha_m \frac{\partial \widehat{\mathbf{Res}}\left(\dot{\mathbf{U}}_{n+\alpha_m,(j)}, \mathbf{U}_{n+\alpha_f,(j)}\right)}{\partial \dot{\mathbf{U}}_{n+\alpha_m}} + \alpha_f\,\delta\,\Delta t_n \frac{\partial \widehat{\mathbf{Res}}\left(\dot{\mathbf{U}}_{n+\alpha_m,(j)}, \mathbf{U}_{n+\alpha_f,(j)}\right)}{\partial \mathbf{U}_{n+\alpha_f}};
\end{aligned} \tag{4.7}$$

3. if, for a prescribed tolerance $tol_R > 0$, the criterion $\dfrac{\|\widehat{\mathbf{Res}}_{n+1,(j)}\|}{\|\widehat{\mathbf{Res}}_{n+1,(0)}\|} \leq tol_R$ is fulfilled, set $\dot{\mathbf{U}}_{n+1} = \dot{\mathbf{U}}_{n+1,(j-1)}$ and $\mathbf{U}_{n+1} = \mathbf{U}_{n+1,(j-1)}$ and terminate the procedure, otherwise continue;

4. solve the linear system:
$$\widehat{\mathbf{K}}_{n+1,(j)}\,\Delta\dot{\mathbf{U}}_{n+1,(j)} = -\widehat{\mathbf{Res}}_{n+1,(j)}; \tag{4.8}$$

5. update the variables:
$$\dot{\mathbf{U}}_{n+1,(j)} = \dot{\mathbf{U}}_{n+1,(j-1)} + \Delta\dot{\mathbf{U}}_{n+1,(j)}, \qquad \mathbf{U}_{n+1,(j)} = \mathbf{U}_{n+1,(j-1)} + \delta\,\Delta t_n\,\Delta\dot{\mathbf{U}}_{n+1,(j)}, \tag{4.9}$$
and return to step 1.

A family of second–order time accurate and unconditionally stable generalized–$\alpha$ methods for linear problems is obtained by choosing $\alpha_m = \frac{1}{2}\left(\frac{3-\rho_\infty}{1+\rho_\infty}\right)$, $\alpha_f = \delta = \frac{1}{1+\rho_\infty}$, where $\rho_\infty \in [0,1]$ governs high frequencies dissipation [31][5]; a typical choice is $\rho_\infty = 0.5$, see e.g. [18, 29, 35].

The time step $\Delta t_n$ can be set as fixed ($\Delta t_n = \Delta t_0$) or determined by an adaptive algorithm. In the latter case, we select an adaptive scheme based on the number of iterations of the multicorrector stage of the generalized–$\alpha$ method (see e.g. [29, 48]); in particular, we set $\Delta t_n = \Delta t_{n-1}\,\chi\sqrt{\frac{j}{j_{ref}+j_0}}$ for $n = 1,\ldots,t_{n_{ts}-1}$ and an initial time step $\Delta t_0$, where $\chi = 1.2$, $j_{ref} = 2$, and $j_0 = 0.8$. As tolerance for the stopping criterion of the multicorretor stage we select $tol_R = 10^{-4}$.

### 4.3 SUPG stabilization for the advection–diffusion PDEs

Since we are interested in solving time dependent advection–diffusion equations in the transport dominated regime, we consider the numerical stabilization of the PDEs in lower dimensional manifolds. In particular, we consider a SUPG stabilization technique similar to the one proposed in [37] for PDEs on surfaces approximated by means of the Finite Element method.

The time dependent linear advection–diffusion problem (3.18) with SUPG stabilization ([9]) reads:
$$\begin{aligned}\text{find } \widehat{u}_h(t) \in \widehat{\mathcal{V}}_{\gamma,h} \;:\; &\widehat{m}\left(\widehat{v}_h, \frac{\partial \widehat{u}_h}{\partial t}(t)\right) + \widehat{a}(\widehat{v}_h, \widehat{u}_h(t)) + \widehat{b}(\widehat{v}_h, \widehat{u}_h(t)) \\ &+\widehat{d}_h(\widehat{v}_h, \widehat{u}_h(t)) - \widehat{q}(\widehat{v}_h) = 0 \qquad \forall \widehat{v}_h \in \widehat{\mathcal{V}}_h,\ \forall t \in (0,T), \\ \text{with } \widehat{u}_h(0) = \widehat{u}_{in,h},&\end{aligned} \tag{4.10}$$

where the form $\widehat{d}_h(\cdot,\cdot)$ represents the SUPG stabilization term. By recalling the definitions (3.20) and (3.21), we define:
$$\widehat{d}_h(\widehat{v}_h, \widehat{w}_h(t)) := \sum_{e=1}^{n_{el}} \int_{\widehat{\Omega}_e} \tau_e\,\widehat{\mathcal{L}}_{adv}\,(\widehat{v}_h)\;\widehat{\mathcal{R}}(\widehat{w}_h(t))\,\widehat{g}\,d\widehat{\Omega}, \tag{4.11}$$

for all $\widehat{v}_h$ and $\widehat{w}_h(t) \in H^2(\widehat{\Omega}_e)$, with $e = 1,\ldots,n_{el}$, and $t \in (0,T)$; the stabilization parameter $\tau_e$ is assumed as piecewise constant over the elements $\widehat{\Omega}_e$[6]. We introduce the characteristic size

[5] The parameter $\rho_\infty$ represents the spectral radius of the amplification matrix of the system for $\Delta t_n \to \infty$.

[6] We notice that in the physical space we have, from Eqs. (3.16) and (3.17), $d_h(v_h, w_h(t)) := \sum_{e=1}^{n_{el}} \int_{\Omega_e} \tau_e\,\mathcal{L}_{adv}\,(v_h)\;\mathcal{R}(w_h(t))\;d\Omega$ for all $v_h$ and $w_h(t) \in H^2(\Omega_e)$, with $e = 1,\ldots,n_{el}$, and $t \in (0,T)$.

(diameter) $h_e$ of the element $\Omega_e$, the characteristic velocity $V_e := \|\widehat{\mathbf{V}}\|_{L^\infty(\widehat{\Omega}_e)}$, the constant $c_p$ depending on the order $p$ of the polynomial approximation[7], and the local Péclet number $\mathbb{P}e_e := \dfrac{V_e\, h_e}{2\mu}$. Following [28, 33, 45], we choose:

$$\tau_e := \frac{1}{2}\left[\frac{1}{\Delta t^2} + \left(\frac{V_e}{h_e}\right)^2 \left(1 + \left(\frac{c_p}{\mathbb{P}e_e}\right)^2\right)\right]^{-1/2}, \tag{4.12}$$

where $\Delta t$ is the time step for the time approximation; we will assume $c_p = p^2$. This choice of $\tau_e$ is obtained by locally approximating the operator $\widehat{\mathcal{L}}^{-1}(\cdot)$, by assuming the use of second order time schemes (as the generalized–$\alpha$ method), and by considering geometrical mappings of the elements $\Omega_e$ from parents domains $(-1,1)^\kappa$; the parameter $\tau_e$ assumes the same form in the parameter and physical spaces.

# 5 Numerical results: PDEs on surfaces

We consider the numerical solution of the problems defined in Sec. 3 for the specific cases of surfaces as lower dimensional manifolds.

## 5.1 The Laplace–Beltrami equation

We numerically solve the Laplace–Beltrami equation (3.10) on two surfaces, we evaluate the errors between the numerical and exact solutions and we estimate the convergence orders of such errors for the polynomial orders $p = 2$ and 3 of the NURBS basis. We recall the definition of the error in $L^2$ norm on a surface, say $err_{L^2} := \|u - u_h\|_{L^2(\Omega)} = \left(\displaystyle\int_\Omega (u - u_h)^2 \, d\Omega\right)^{1/2}$, and the error in $H^1$ norm, reading $err_{H^1} := \|u - u_h\|_{H^1(\Omega)} = \left(err_{L^2}^2 + \displaystyle\int_\Omega |\nabla_\Omega (u - u_h)|^2 \, d\Omega\right)^{1/2}$.

Firstly, we consider as computational domain $\Omega$ a quarter of the cylinder represented in Fig. 2(left) (corresponding to the quadrant with $\mathrm{x} \geq 0$ and $\mathrm{y} \geq 0$) with unitary radius and height $L$. We choose $\mu = 1$ and $f(\phi, z) = \beta \left(\dfrac{\alpha^2\pi^2}{L^2} g_{\phi,1}(\phi) - g_{\phi,2}(\phi)\right) g_{\mathrm{z}}(\mathrm{z})$, where $\phi := \mathrm{atan}\left(\dfrac{\mathrm{x}}{\mathrm{y}}\right)$, $g_{\phi,1}(\phi) := (1 - \cos(\phi))\,(1 - \sin(\phi))$, $g_{\phi,2}(\phi) := (\cos(\phi) + \sin(\phi) - 4\,\sin(\phi)\,\cos(\phi))$, and $g_{\mathrm{z}}(\mathrm{z}) := \sin\left(\alpha\,\pi\,\dfrac{\mathrm{z}}{L}\right)$ for $\alpha \in \mathbb{N}_0$ and $\beta > 0$; then, we set $u(\mathbf{x}) = \gamma(\mathbf{x}) = 0$ on $\Gamma$. The exact solution of the problem reads $u(\phi, \mathrm{z}) = \beta\, g_{\phi,1}(\phi)\, g_{\mathrm{z}}(\mathrm{z})$ in cylindrical coordinates. Specifically, we select $\alpha = 3$, $\beta = 1/\left(3/2 - \sqrt{2}\right)$, and $L = 4$. We solve the problem by meas of Isogeometric Analysis with NURBS basis functions of order $p = 2$ and $p = 3$ for different "mesh" sizes starting from a mesh with 2 elements in the circumferential direction. The exact and numerical solution and corresponding "meshes" are reported in Fig. 3; we highlight the smoothness of the approximated solutions in circumferential direction even for a small number of "mesh" elements. The convergence rates of the errors are reported in Fig. 4 for the polynomial orders $p = 2$ and 3; in particular, we obtain the convergence rates $p + 1$ and $p$ for the norms $L^2$ and $H^1$, respectively. Based on these results, we highlight the agreement

[7] The constant $c_p$ stems from an inverse inequality of the type $\|\Delta_\Omega v_h\|_{L^2(\Omega_e)} \leq \dfrac{c_p}{h_e} \|v_h\|_{L^2(\Omega_e)}$ for all $v_h \in \mathcal{V}_h$ and $e = 1, \ldots, n_{el}$.

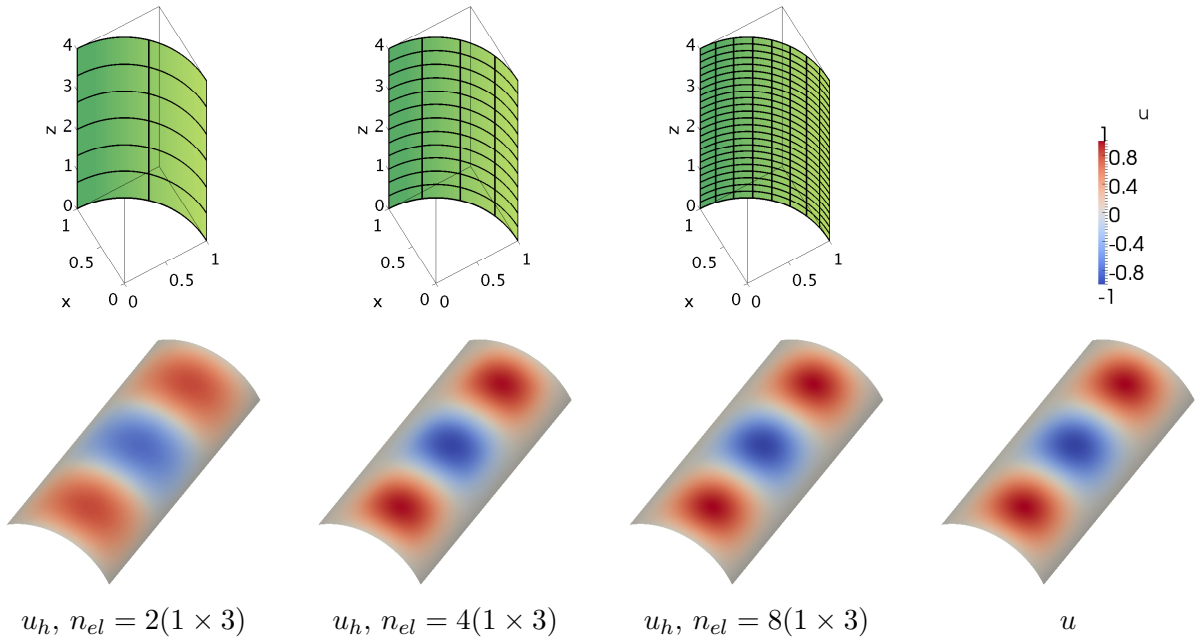


Figure 3: Laplace–Beltrami problem on a cylindrical shell. Refined meshes (top), corresponding numerical solutions $u_h$ (bottom), and exact solution $u$ (bottom–right).

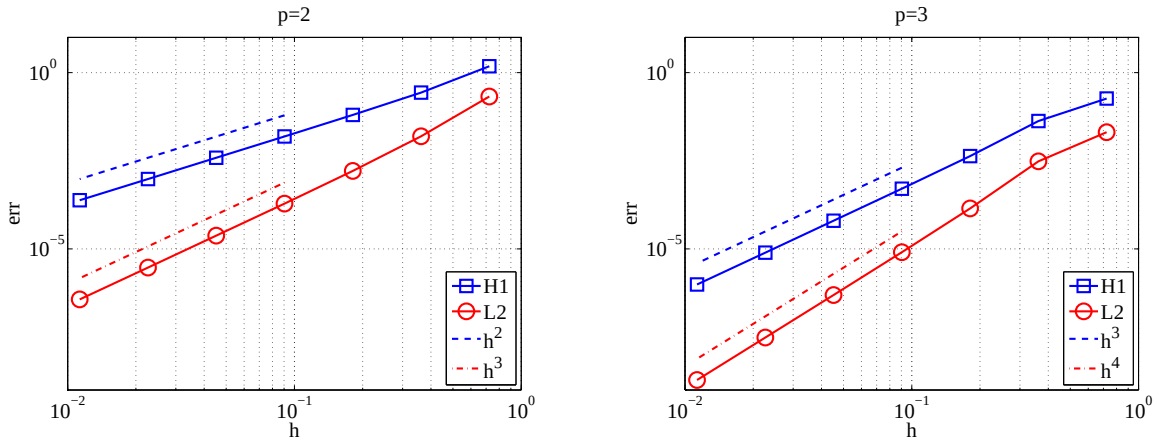


Figure 4: Laplace–Beltrami problem on a cylindrical shell. Convergence of the errors $err_{H^1}$ (—□) and $err_{L^2}$ (—○) and reference convergences rates $p$ (- -) and $p+1$ (. -) vs. the "mesh" size $h$ for $p = 2$ (left) and $p = 3$ (right).

of the convergences rates with the expected theoretical ones in the sense discussed in the following Remark 5.1.

**Remark 5.1.** *Even if in this work we do not provide a rigorous proof for the convergence rates of the errors under "mesh" refinement, we speculate that the a priori error estimates provided in [2] could be extended and generalized to the case of second order PDEs defined on lower dimensional*

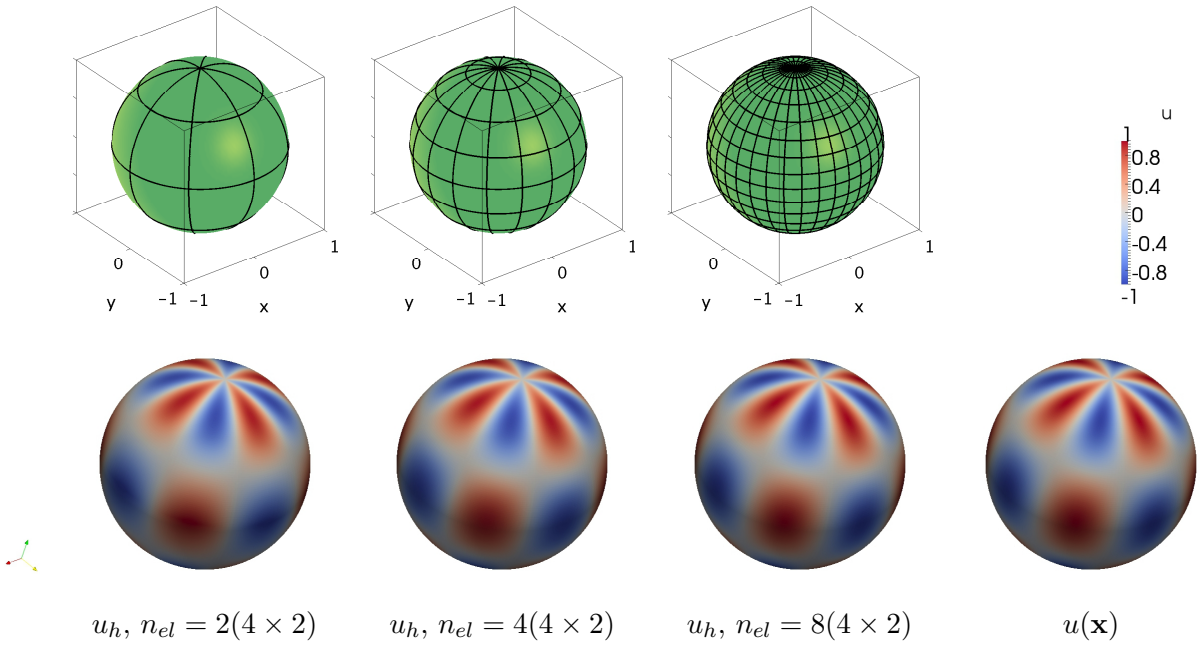


Figure 5: Laplace–Beltrami problem on a sphere. Refined meshes (top), corresponding numerical solutions $u_h$ (bottom), and exact solution $u$ (bottom–right).

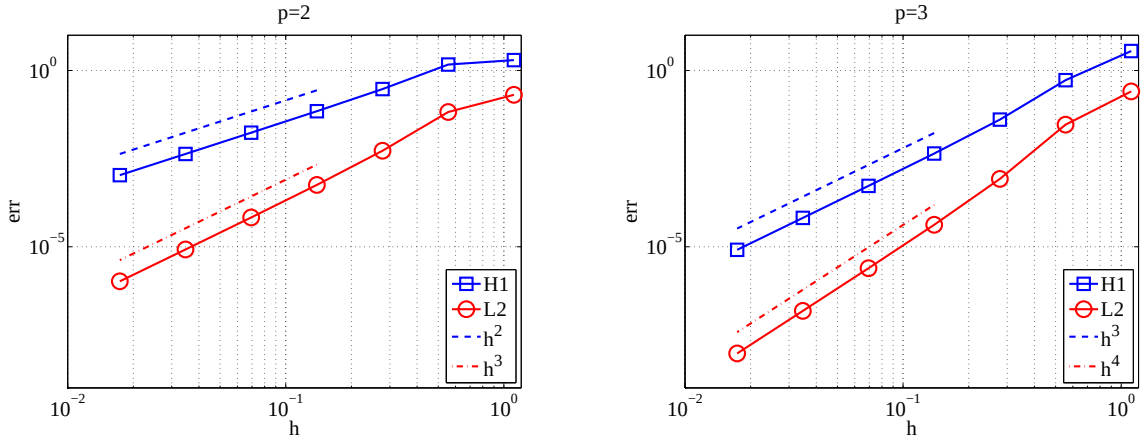


Figure 6: Laplace–Beltrami problem on a sphere. Convergence of the errors $err_{H^1}$ (—□) and $err_{L^2}$ (—○) and reference convergences rates $p$ (- -) and $p+1$ (. -) vs. the "mesh" size $h$ for $p = 2$ (left) and $p = 3$ (right).

*manifolds, provided that suitable regularity hypotheses on the geometrical mappings hold.*

Then, we consider a Laplace–Beltrami problem with exact solution on the sphere of unitary radius reported in Fig. 2(right); since the surface is closed ($\Gamma \equiv \emptyset$), we impose the constraint $\int_\Omega u \, d\Omega = 0$. We set $f(\phi,\theta) = \sin(\alpha\phi)\sin(\beta\theta)\left[\dfrac{\alpha^2}{\sin^2(\theta)} + \beta^2 - \beta\,\dfrac{\cos(\theta)\,\cos(\beta\theta)}{\sin(\theta)\,\sin(\beta\theta)}\right]$ with

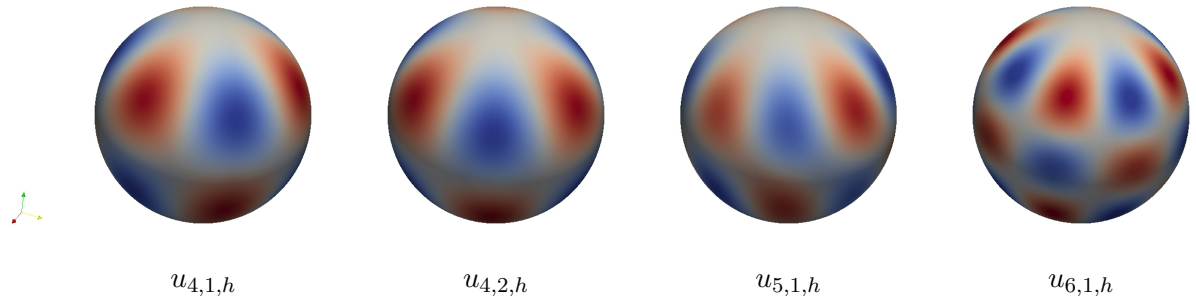

$u_{4,1,h}$ $u_{4,2,h}$ $u_{5,1,h}$ $u_{6,1,h}$

Figure 7: Eigenvalue problem on a sphere. Eigenfunctions $u_{4,1,h}$, $u_{4,2,h}$, $u_{5,1,h}$, and $u_{6,1,h}$ (from left to right).

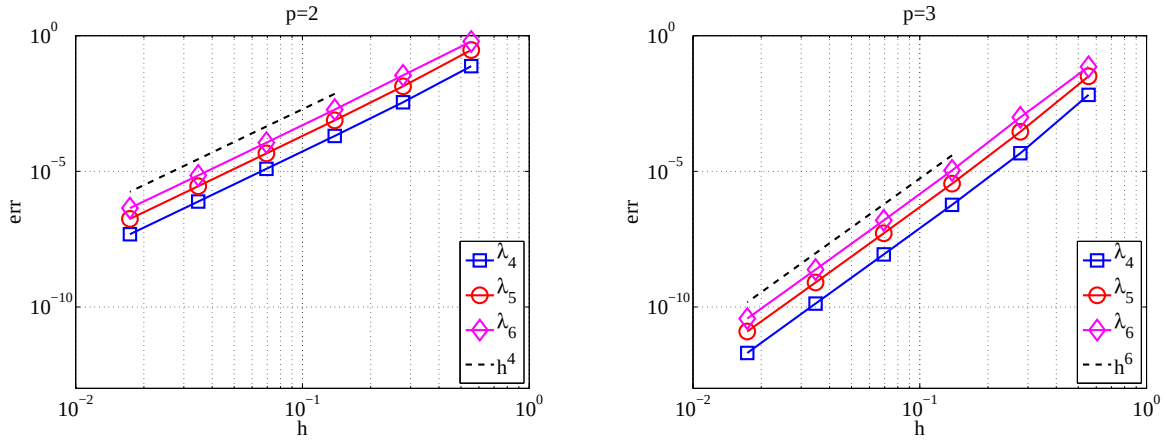


Figure 8: Eigenvalue problem on a sphere. Convergence of the errors $err_n$ on the eigenvalues $\lambda_n$ for $n = 4$ (—□), $n = 5$ (—○), and $n = 6$ (—◇) and reference convergences rate $2p$ (- -) for $p = 2$ (left) and $p = 3$ (right).

$\phi := \text{atan2}\left(\frac{\text{x}}{\text{y}}\right)$, $\theta := \text{acos}\left(\frac{\text{z}}{\text{r}}\right)$, $\alpha > 0$, $\beta > 0$, and $\mu = 1$. The exact solution in spherical coordinates reads $u(\phi, \theta) = \sin(\alpha\phi)\sin(\beta\theta)$. In particular, we choose $\alpha = 3$ and $\beta = 4$. We report in Fig. 5 the exact and numerical solutions corresponding to "meshes" progressively refined; we remark the smoothness of the numerical solution along both the parametric directions even for the coarsest "meshes". In Fig. 6 we highlight the convergence orders of the errors $err_{L^2}$ and $err_{H^1}$ which are in agreement with the theoretical ones (see Remark 5.1).

### 5.2 The eigenvalue problem

We consider the numerical approximation of the eigenvalue problem (3.12) associated to the Laplace–Beltrami operator on the sphere of unitary radius of Fig. 2(right). The exact values of the eigenvalues are $\lambda_n = n(n+1)$, each with multiplicity $2n+1$, for $n = 0, 1, \ldots, \infty$ (see e.g. [42]), to which correspond the eigenfunctions $u_{n,l_n}$, with $l_n = 1, \ldots, 2n+1$. We numerically approximate the problem by means of Isogeometric Analysis on a "mesh" with $n_{el} = 131,072$ elements and basis

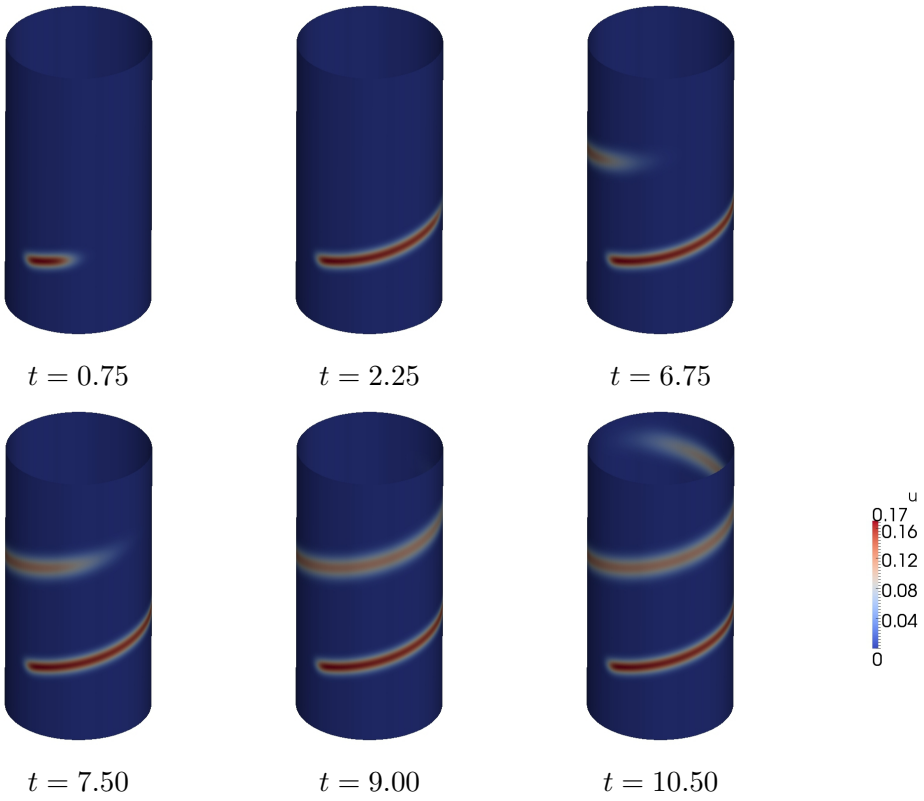


Figure 9: Time dependent advection–diffusion problem on a cylindrical shell. Evolution of the solution in time.

functions of order $p = 2$; in Fig. 7 we report for example the computed eigenfunctions $u_{4,1,h}$, $u_{4,2,h}$, $u_{5,1,h}$, and $u_{6,1,h}$ corresponding to the eigenvalues $\lambda_4 = 20$, $\lambda_5 = 30$, and $\lambda_6 = 42$, respectively. In Fig. 8 we report the errors on the eigenvalues $\lambda_4$, $\lambda_5$, and $\lambda_6$, say $err_n := |\lambda_n - \lambda_{n,h}|$, vs. the "mesh" size $h$ when considering basis functions of order $p = 2$ and $p = 3$. As expected by the theory for second order spatial operators [46], the convergence orders obtained for the numerical results correspond to $2p$ for the "smaller" eigenvalues of the spectrum (see Remark 5.1).

### 5.3 The time dependent linear advection–diffusion equation

We consider the time dependent linear advection–diffusion equation on the cylindrical shell reported in Fig. 2(left). By using the notation of Sec. 3.4 and using cylindrical coordinates, we set $\mathbf{V}(\phi, \mathrm{z}) = \dfrac{V_0}{\sqrt{1+a^2}}(\widehat{\boldsymbol{\phi}} + a\widehat{\mathbf{z}})$, and $f(\phi, \mathrm{z}) = e^{-b\left((\phi-\phi_0)^2+(z-z_0)^2\right)}$, where $\phi := \mathrm{atan2}\begin{pmatrix}\mathrm{x}\\ \mathrm{y}\end{pmatrix}$, $V_0$, $a$, $\phi_0$, and $z_0 \in \mathbb{R}$; we set homogeneous Neumann conditions on the boundary $\Gamma = \Gamma_N$ and $u_{in}(\mathbf{x}) = 0$. In particular, we set $\mu = 5.0 \cdot 10^{-4}$, $V_0 = 1$, $a = 0.2$, $b = 100$, $\phi_0 = \dfrac{\pi}{4}$, and $z_0 = 0.5$. We numerically solve the problem by means of Isogeometric Analysis with the SUPG stabilization technique discussed in Sec. 4.3. A NURBS representation with basis of order $p = 2$ and comprised of $n_{el} = 12,288$ "mesh" elements is considered. For the time discretization, the generalized–$\alpha$ method of Sec. 4.2 is used with the fixed time step $\Delta t_0 = 1.5 \cdot 10^{-2}$. In Fig. 9 we report the evolution of the solution in

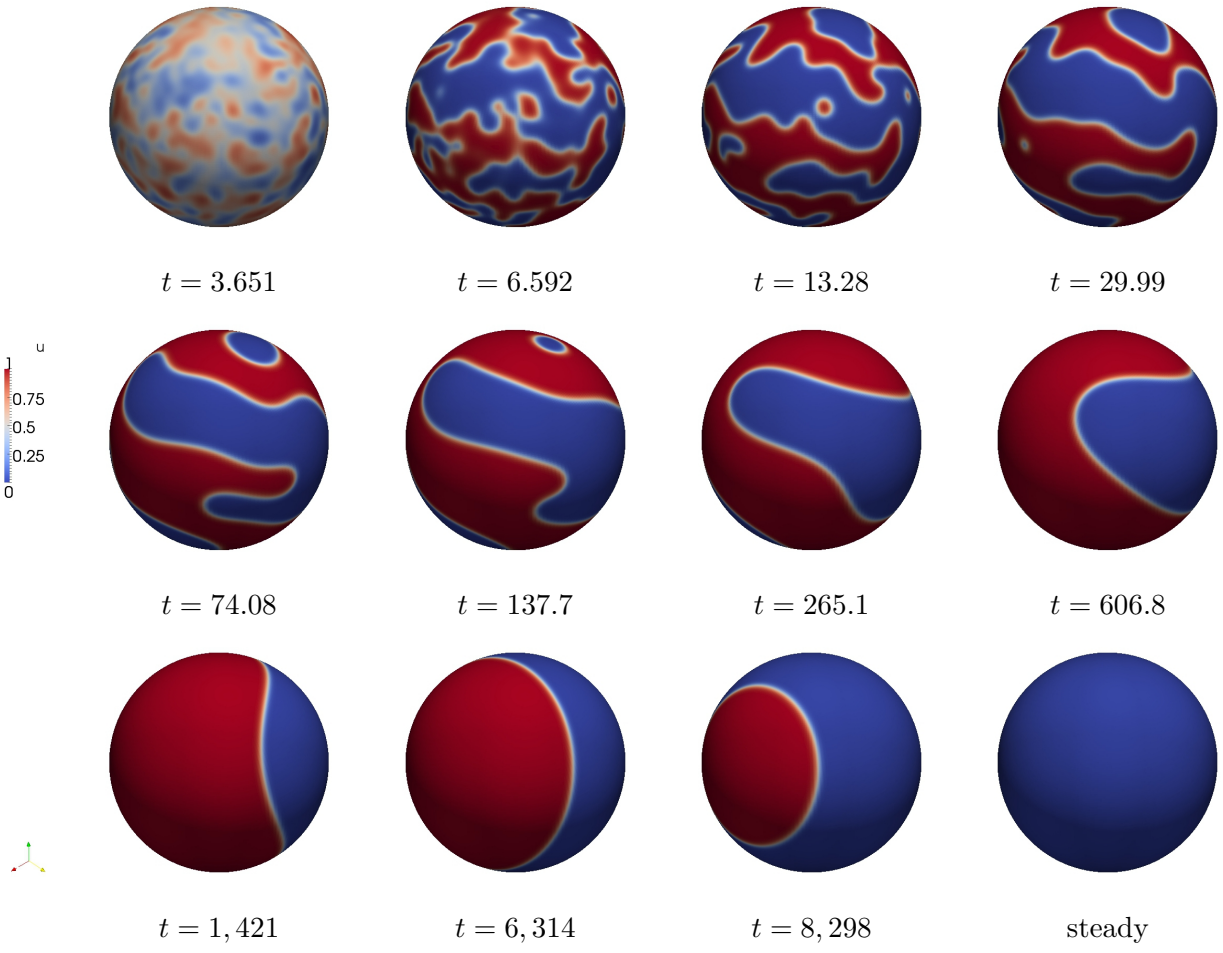


Figure 10: Cahn–Allen equation on a sphere. Evolution of the solution in time.

time; we highlight its helical distribution along the surface of the cylindrical shell induced by the advective field.

### 5.4 The Cahn–Allen problem

We solve the Cahn–Allen problem defined in Sec. 3.5 on the sphere of unitary radius of Fig. 2(right). By using the notation of Sec. 3.5, we select $\mu = 5.0 \cdot 10^{-4}$ and $u_{in} = u_0 + \varepsilon$, where $u_0 = 0.5$ and $\varepsilon$ is a random distribution such that $|\varepsilon| \leq 0.1$. We numerically solve the problem by means of Isogeometric Analysis with NURBS basis functions of order $p = 2$ and a "mesh" comprised of $n_{el} = 32,768$ elements; the time approximation is based on the generalized–$\alpha$ method with the adaptive time stepping scheme initialized with the time step $\Delta t_0 = 5.0 \cdot 10^{-1}$. In Fig. 10 we report the evolution of the concentration $u(\mathbf{x}, t)$ in time. The phase transition evolves towards the steady state to a configuration with the phases fully separated with a minimum perimeter interface. However, due to the fact that the Cahn–Allen equation does not represent a mass conservative system, the solution evolves to a pure phase at the steady state, which corresponds to $u = 0$ in

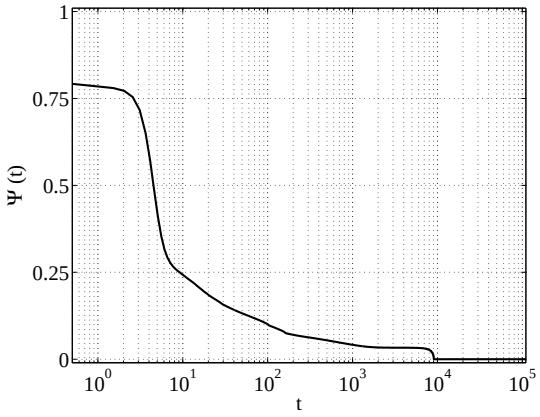


Figure 11: Cahn–Allen equation on a sphere. Evolution of the free energy $\widetilde{\Psi}(t)$ in time.

the case under consideration, since $\int_\Omega u_{in}\, d\Omega < u_0 = 0.5$. In Fig. 11 we report the evolution of the (Liapunov) free energy functional $\widetilde{\Psi}(t)$ for which we observe that $\dfrac{d\widetilde{\Psi}}{dt}(t) \leq 0$.

# 6 Conclusions

In this work we showed the efficacy of Isogeometric Analysis for the numerical approximation of PDEs defined on lower dimensional manifolds, specifically on surfaces. We considered different linear and nonlinear, elliptic and parabolic PDEs with second order spatial operators of the Laplace–Beltrami type; examples include the eigenvalue problem, the time dependent advection–diffusion equation, and the Cahn–Allen equation. We highlighted the capability of Isogeometric Analysis of facilitating the encapsulation of the exact surface representations in the analysis at their coarsest level of discretization, especially for geometries as cylindrical and spherical shells represented by NURBS. Specifically, the convergence orders of the errors for benchmark tests cases highlight the effect of the accurate geometrical description on the computation of the numerical solutions.

# Acknowledgements

We acknowledge Mr. Dmitry Alexeev for providing some preliminary insights into the topic and Ms. Claudia Colciago for the fruitful discussions.

# References

[1] M. Berger. *A Panoramic View of Riemannian Geometry*. Springer–Verlag, Berlin and Heidelberg, 2003.

[2] Y. Bazilevs, L. Beirão da Veiga, J.A. Cottrell, T.J.R. Hughes, and G. Sangalli. Isogeometric Analysis: approximation, stability, and error estimates for $h$–refined meshes. *Mathematical Models and Methods for Applied Sciences* **16**(7):1031–1090, 2006.

[3] Y. Bazilevs, V.M. Calo, J.A. Cottrell, T.J.R. Hughes, A. Reali, and G. Scovazzi. Variational multiscale residual–based turbulence modeling for large eddy simulation of incompressible flows. *Computer Methods in Applied Mechanics and Engineering* **197**(1–4):173–201, 2007.

[4] L. Beirão da Veiga, A. Buffa, J. Rivas, and G. Sangalli. Some estimates for $h-p-k$–refinement in Isogeometric Analysis. *Numerische Mathematik* **118**(2):271–305, 2011.

[5] M. Beltramío, L.–T. Cheng, S. Osher, and G. Sapiro. Variational problems and partial differential equations on implicit surfaces. *Journal of Computational Physics* **174**(2): 759-780, 2001.

[6] D.J. Benson, Y. Bazilevs, M.C. Hsu, and T.J.R. Hughes. Isogeometric shell analysis: the Reissner-Mindlin shell. *Computer Methods in Applied Mechanics and Engineering* **199**(5–8):276–289, 2010.

[7] A. Bonito, R.H. Nochetto, and S.M. Pauletti. Dynamics of biomembranes: effect of the bulk fluid. *Mathematical Modelling of Natural Phenomena* **6**(5):25–43, 2011.

[8] A. Bonito, R.H. Nochetto, and S.M. Pauletti. Geometrically consistent mesh modification. *SIAM Journal on Numerical Analysis* **48**(5):1877–1899, 2010.

[9] A.N. Brooks and T.J.R. Hughes. Streamline upwind/Petrov–Galerkin formulations for convection dominated flows with particular emphasis on the incompressible Navier–Stokes equations. *Computer Methods in Applied Mechanics and Engineering* **32**(1–3):199–259, 1982.

[10] J.W. Cahn. On spinodal decomposition. *Acta Metallurgica* **9**(9):795-801, 1961.

[11] J.W. Cahn and J.E. Hilliard. Free energy of a non–uniform system. I. Interfacial free energy. *Journal of Chemical Physics* **28**(2):258–267, 1958.

[12] W.C. Carter, J. Taylor, and J.W. Cahn. Variational methods for microstructural-evolution theories. *JOM Journal of the Minerals, Metals and Materials Society* **49**(12):30-36, 1997.

[13] J. Chung and G.M. Hulbert. A time integration algorithm for structural dynamics with improved numerical dissipation: the generalized $\alpha$–method. *Journal of Applied Mechanics* **60**(2):371–375, 1993.

[14] Ph. G. Ciarlet. *The Finite Element Method for Elliptic Problems*. North–Holland, 1978.

[15] S. Coriasco, E. Schrohe, and J. Seiler. Differential operators on conic manifolds: maximal regularity and parabolic equations. *Bullettin de la Société Royale de Sciences de Liège* **70**(4–6):207–229, 2001.

[16] J.A. Cottrell, T.J.R. Hughes, and Y. Bazilevs. *Isogeometric Analysis: toward integration of CAD and FEA*. Wiley, 2009.

[17] J.A. Cottrell, T.J.R. Hughes, and A. Reali. Studies of refinement and continuity in isogeometric structural analysis. *Computer Methods in Applied Mechanics and Engineering* **196**(41–44):4160–4183, 2007.

[18] L. Dedè, M.J. Borden, and T.J.R. Hughes. Topology optimization with Isogeometric Analysis in a phase field approach. *Archives in Computational Methods in Engineering* **19**(3):427–465, 2012.

[19] M.C. Delfour and J.–P. Zolésio. *Shapes and Geometries: Analysis, Differential Calculus, and Optimization*. Advances in Design and Control 4, SIAM, Philadelphia, PA, 2001.

[20] G. Dziuk. Finite elements for the Beltrami operator on arbitrary surfaces. In *Partial differential equations and calculus of variations*, 142–155, Lecture Notes in Mathematics **1357**, 1988.

[21] G. Dziuk and C.M. Elliott. Eulerian finite element method for parabolic PDEs on implicit surfaces. *Interfaces and Free Boundaries* **10**:119-138, 2008.

[22] G. Dziuk and C.M. Elliott. Surface finite elements for parabolic equations. *Journal of Computational Mathematics* **25**(4):385–407, 2007.

[23] C.M. Elliott and H. Garcke. Existence results for diffusive surface motion laws. *Advances and Applications in Mathematical Sciences* **7**(1):465–488, 1997.

[24] C.M. Elliott and H. Garcke. On the Cahn–Hilliard equation with degenerate mobility. *SIAM Journal on Mathematical Analysis* **27**(2):404–423, 1996.

[25] J. Escher, U.F. Mayer, and G. Simonett. The surface diffusion flow for immersed hypersurfaces. *SIAM Journal on Mathematical Analysis* **29**(6):1419–1433, 1998.

[26] J.A. Evans, Y. Bazilevs, I. Babuška, and T.J.R. Hughes. $n$–widths, sup–infs, and optimality ratios for the $k$–version of the Isogeometric finite element method. *Computer Methods in Applied Mechanics and Engineering* **198**(21–26):1726–1741, 2009.

[27] P.C. Fife. Models for phase separation and their mathematics. *Electronic Journal of Differential Equations* **48**:1-26, 2000.

[28] L.P. Franca, S.L. Frey, T.J.R. Hughes. Stabilized finite element methods: I. Application to the advective–diffusive model. *Computer Methods for Applied Mechanics in Engineering* **95**(2):253–276, 1992.

[29] H. Gomez, V.M. Calo, Y. Bazilevs, and T.J.R. Hughes. Isogeometric analysis of the Cahn-Hilliard phase-field model. *Computer Methods for Applied Mechanics in Engineering* **197**(49–50):4333–4352, 2008.

[30] J.B. Greer, A.L. Bertozzi, and G. Sapiro. Fourth order partial differential equations on general geometries. *Journal of Computational Physics* **216**(1):216–246, 2006.

[31] T.J.R. Hughes. *The Finite Element Method: Linear Static and Dynamic Finite Element Analysis*. Dover Publications, Mineola, 2000.

[32] T.J.R. Hughes, J.A. Cottrell, and Y. Bazilevs. Isogeometric analysis: CAD, finite elements, NURBS, exact geometry and mesh refinement. *Computer Methods in Applied Mechanics and Engineering* **194**(39–41):4135–4195, 2005.

[33] T.J.R. Hughes, G. Scovazzi, and L.P. Franca. Multiscale and stabilized methods. In *Encyclopedia of Computational Mechanics*, E. Stein, R. de Borst, and T.J.R. Hughes (eds.). John Wiley & Sons, 2004.

[34] K.E. Jansen, C.H. Whiting, and G.M. Hulbert. A generalized–$\alpha$ method for integrating the filtered Navier-Stokes equations with a stabilized finite element method. *Computer Methods in Applied Mechanics and Engineering* **190**(3–4):305–319, 2000.

[35] J. Liu, L. Dedè, J.A. Evans, M.J. Borden, and T.J.R. Hughes. Isogeometric Analysis of the advective Cahn–Hilliard equation: spinodal decomposition under shear flow. *ICES report, The University of Texas at Austin* **12–12**, 2012. `http://www.ices.utexas.edu`

[36] K. Mekchay, P. Morin, and R.H. Nochetto. AFEM for the Laplace–Beltrami operator on graphs: design and conditional contraction property. *Mathematics of Computations* **80**(274):625–648, 2011.

[37] M.A. Olshanskii, A. Reuskeny, and X. Xu. A stabilized Finite Element method for advection–diffusion equations on surfaces. *Institut für Geometrie und Praktische Mathematik, RWTH Aachen, Preprint* **344**, 2012. `http://www.igpm.rwth-aachen.de`

[38] L. Piegl and W. Tiller. *The NURBS Book*. Springer–Verlag, New York, 1997.

[39] A. Quarteroni, R. Sacco, and F. Saleri. *Numerical Mathematics*. Springer, Berlin and Heidelberg, 2007.

[40] A. Quarteroni and A. Valli. *Numerical Approximation of Partial Differential Equations*. Springer–Verlag, Berlin, Heidelberg, 1994.

[41] A. Rätz and A. Voigt. PDE's on surfaces – a diffuse interface approach. *Communications in Mathematical Sciences* **4**(3):575–590, 2006.

[42] M. Reuter, F.–E. Wolter, M. Shenton, and M. Niethammer. Laplace–Beltrami eigenvalues and topological features of eigenfunctions for statistical shape analysis. *Journal Computer–Aided Design* **41**(10):739–755, 2009.

[43] M.A. Scott, R.N. Simpson, J.A. Evans, S. Lipton, S.P.A. Bordas, T.J.R. Hughes, and T.W. Sederberg. Isogeometric boundary element analysis using unstructured T–splines. *ICES report, The University of Texas at Austin* **12–23**, 2012. `http://www.ices.utexas.edu`

[44] T.W. Sederberg, J.M. Zhengs, and J.M. Bakenov. T–splines and T–NURCCSs. *ACM Transactions on Graphics* **22**(3):477–484, 2003.

[45] F. Shakib, T.J.R. Hughes, and Z. Johan. A new finite element formulation for computational fluid dynamics: X. The compressible Euler and Navier–Stokes equations. *Computer Methods in Applied Mechanics and Engineering* **89**(1–3):141–219, 1991.

[46] G. Strang and G.J. Fix. *An Analysis of the Finite Element Method*. Prentice–Hall, Inc., Englewood Cliffs, N.J., 1973.

[47] S.P. Timoshenko and S. Woinowsky–Krieger. *Theory of Plates and Shells*. McGraw–Hill, New York, 1959.

[48] O. Wodo and B. Ganapathysubramanian. Computationally efficient solution to the Cahn-Hilliard equation: adaptive implicit time schemes, mesh sensitivity analysis and the 3D isoperimetric problem. *Journal of Computational Physics* **230**(15):6037–6080, 2011.

[49] L.C. Wrobel and M.H. Aliabadi. *The Boundary Element Method*. Wiley, Chichester, 2002.

**Recent publications :**

**MATHEMATICS INSTITUTE OF COMPUTATIONAL SCIENCE AND ENGINEERING**
**Section of Mathematics**
**Ecole Polytechnique Fédérale**
**CH-1015 Lausanne**

**23.2012** P. CHEN, A. QUARTERONI, G. ROZZA:
*Stochastic optimal Robin boundary control problems of advection-dominated elliptic equations*

**24.2012** J. BECK, F. NOBILE, L. TAMELLINI, R. TEMPONE:
*Convergence of quasi-optimal stochastic Galerkin methods for a class of PDES with random coefficients*

**25.2012** E. FAOU, F. NOBILE, C. VUILLOT:
*Sparse spectral approximations for computing polynomial functionals*

**26.2012** G. ROZZA, A. MANZONI, F. NEGRI:
*Reduction strategies for PDE-constrained optimization problems in haemodynamics*

**27.2012** C. EFFENBERGER:
*Robust successive computation of eigenpairs for nonlinear eigenvalue problems*

**28.2012** C. LUBICH, T. ROHWEDDER, R. SCHNEIDER, B. VANDEREYCKEN:
*Dynamical approximation of hierarchical Tucker and tensor-train tensors*

**29.2012** A. ABDULLE, Y. BAI:
*Adaptive reduced basis finite element heterogeneous multiscale method*

**30.2012** L. KARLSSON, D. KRESSNER:
*Optimally packed chains of bulges in multishift QR algorithms*

**31.2012** F. BONIZZONI, A. BUFFA, F. NOBILE:
*Moment equations for the mixed formulation of the Hodge Laplacian with stochastic data*

**32.2012** M. MOTAMED, F. NOBILE, R. TEMPONE:
*Analysis and computation of the elastic wave equation with random coefficients*

**33.2012** T. LASSILA, A. MANZONI, A. QUARTERONI, G. ROZZA:
*Generalized reduced basis methods and n-width estimates for the approximation of the solution manifold of parametric PDEs*

**34.2012** P.CHEN, A. QUARTERONI, G. ROZZA:
*Comparison between reduced basis and stochastic collocation methods for elliptic problems*

**35.2012** A. ABDULLE, G. VILMART, K.C. ZYGALAKIS:
*Mean-square A-stable diagonally drift-implicit integrators of weak second order for stiff Itˆo stochastic differential equations*

**36.2012** L. DEDÈ, A. QUARTERONI:
*Isogeometric analysis for second order partial differential equations on surfaces*